MCB Accepted Manuscript Posted Online 3 October 2016
Mol. Cell. Biol. doi:10.1128/MCB.00411-16

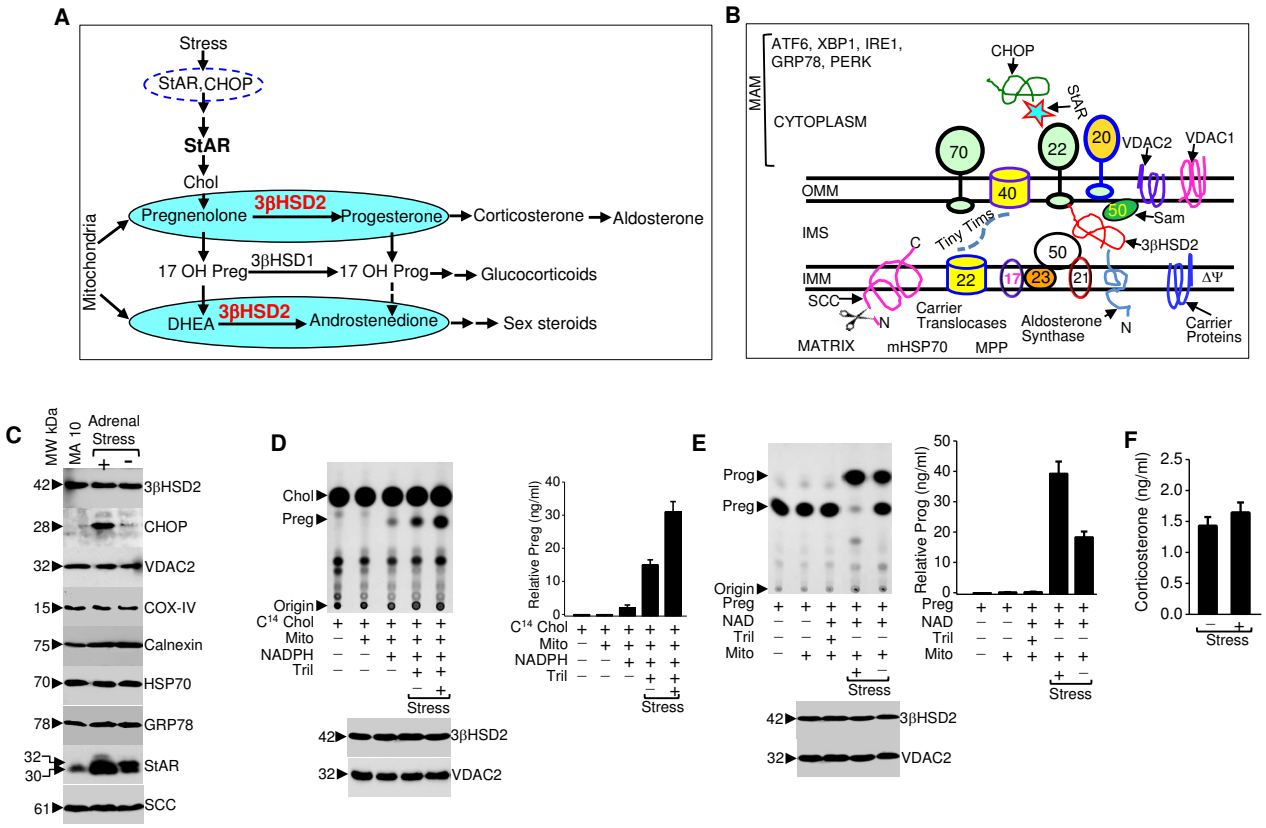

Figure 1

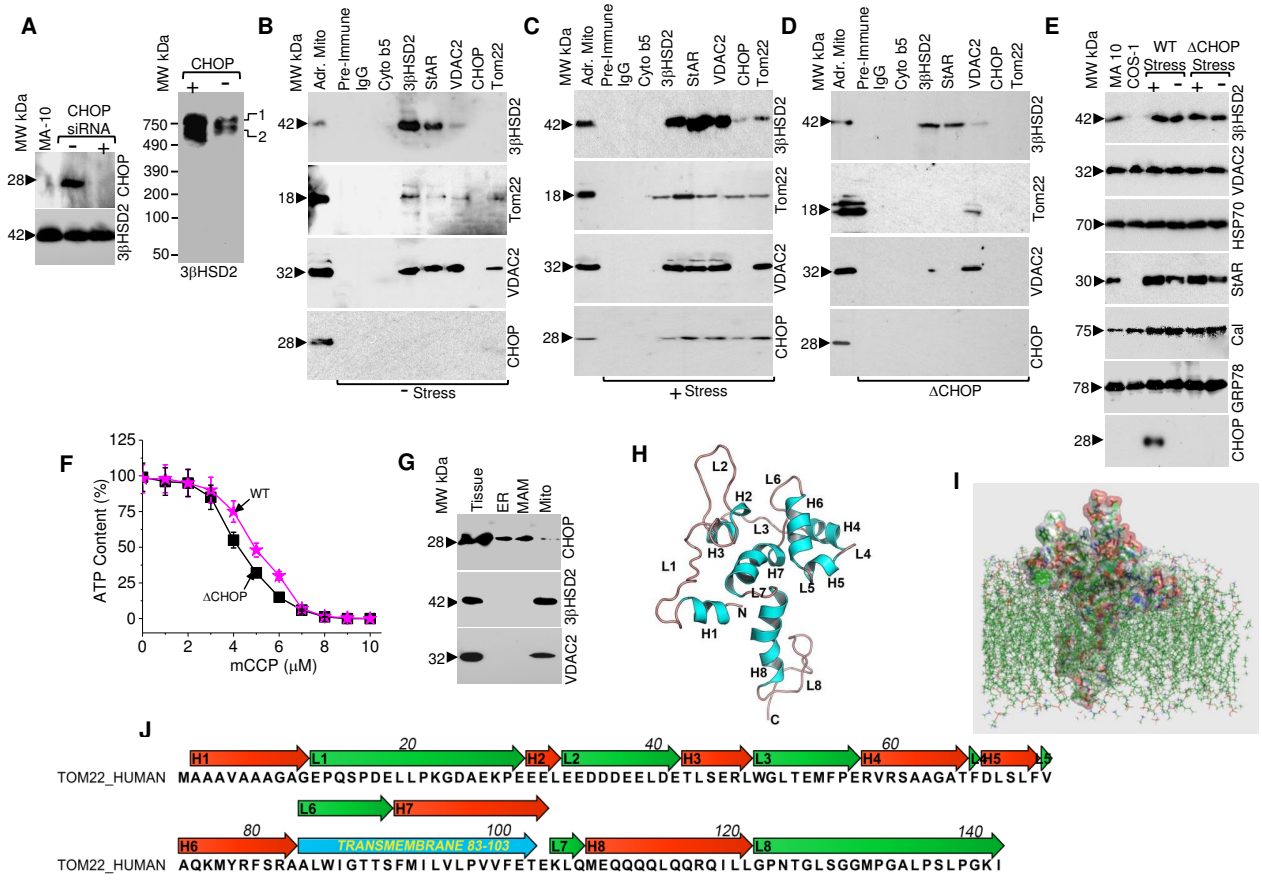

Figure 2

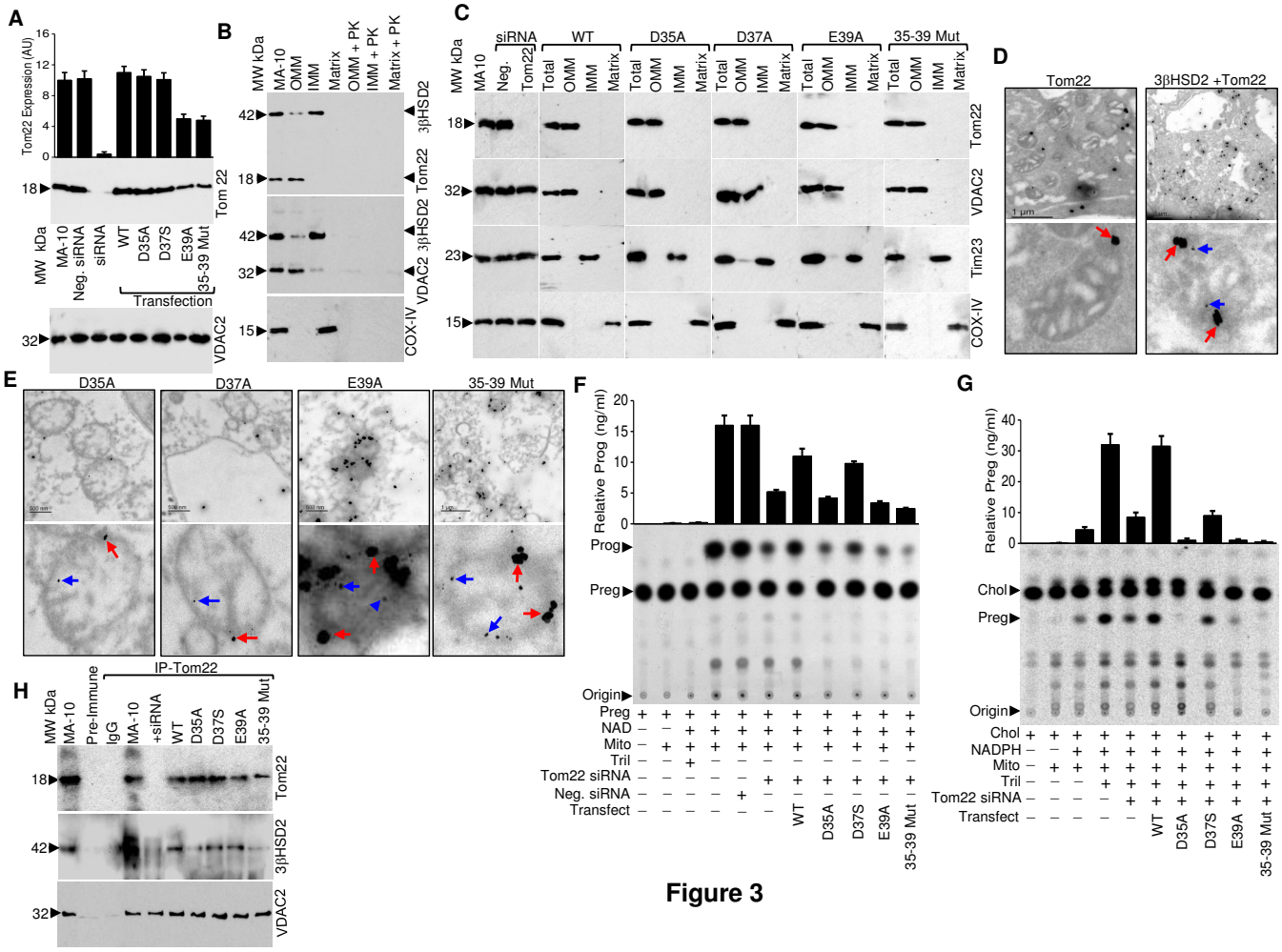

Figure 3

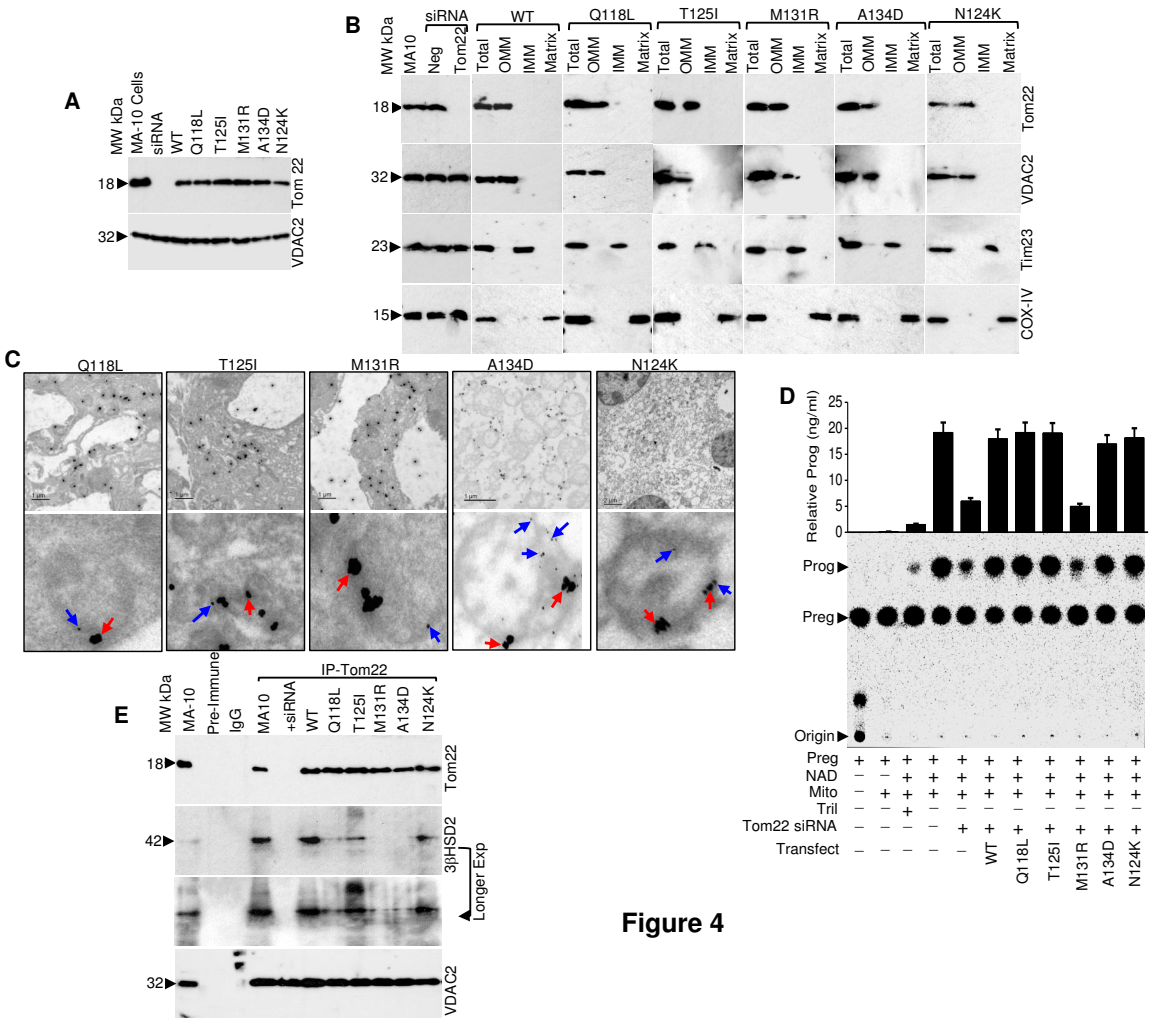

Figure 4

Figure 5

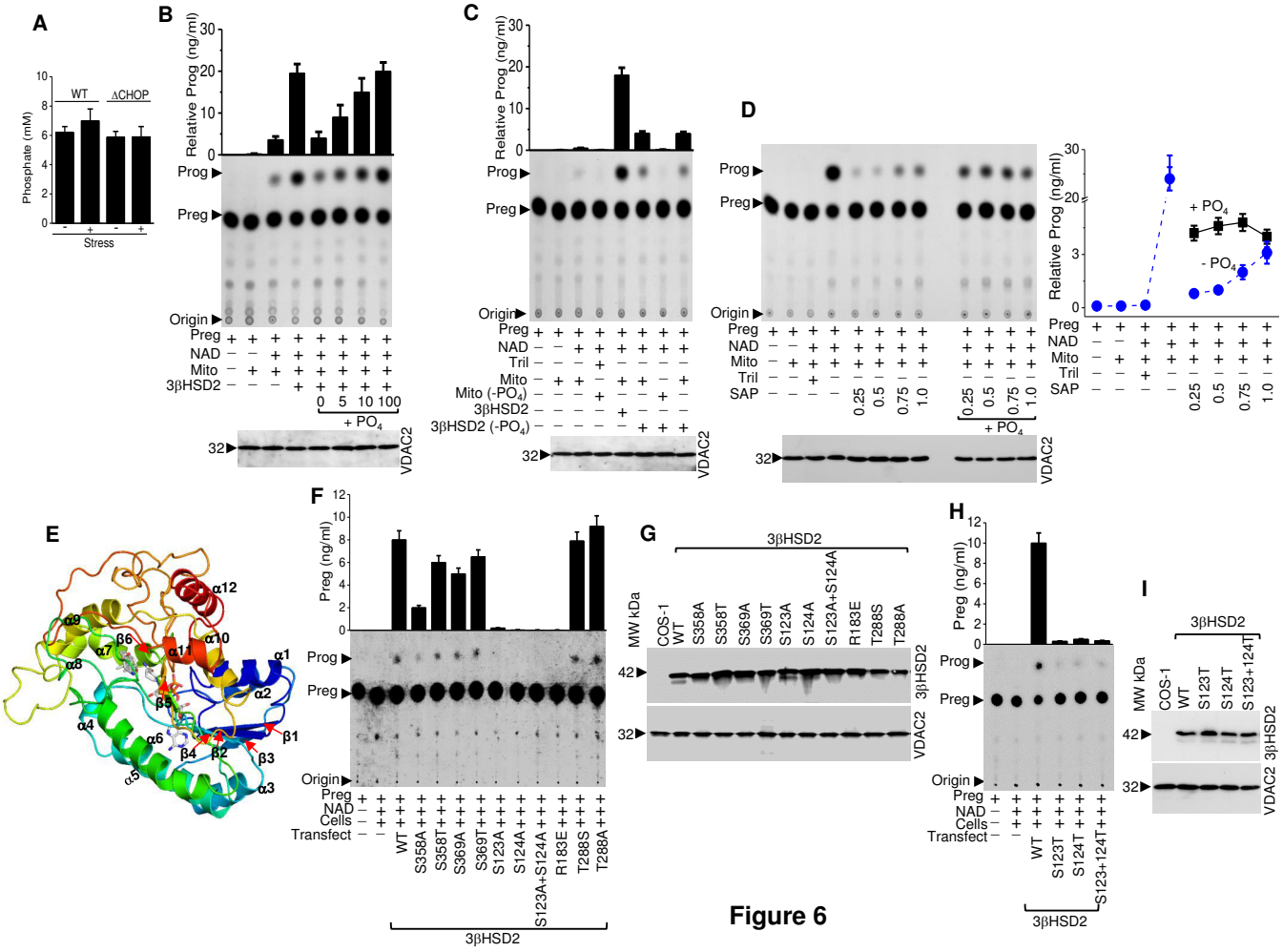

Figure 6

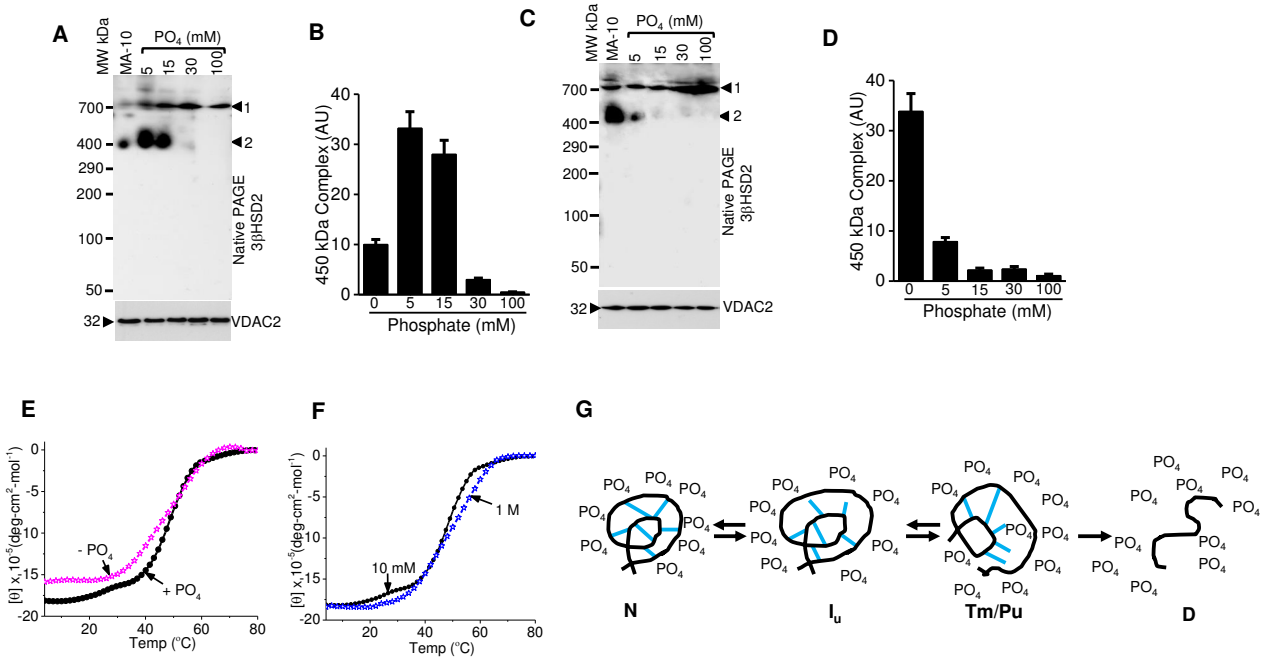

Figure 7

MCB 00411-16R1

Endoplasmic reticulum stress enhances mitochondrial metabolic activity in mammalian adrenals and gonads

Manoj Prasad[1], Anna N. Walker[2], Jasmeet Kaur [1,6], James L. Thomas[3], Shirley A. Powell[3], Amit V. Pandey[4], Randy M. Whittal[5], William E. Burak[1,6], Guy Petruzzelli[1,6], Himangshu S. Bose[1,6*]

[1]Laboratory of Biochemistry and Cell Biology, Biomedical Sciences, Mercer University School of Medicine, Savannah, GA 31404, USA; [5]Department of Chemistry, University of Alberta, Edmonton, Alberta, Canada; [3]Division of Basic Medical Sciences, Mercer University School of Medicine, Macon, GA 31207, USA; [2]Department of Pathology, Mercer University School of Medicine, Macon, GA 31207, USA. [4]Pediatric Endocrinology Diabetology & Metabolism, University Children's Hospital Bern, Freiburgstrasse 15, Bern 3010, Switzerland; and [6]Memorial University Medical Center, Anderson Cancer Institute, Savannah, GA 31404, USA.

Running Title: Stress facilitates mitochondrial metabolism

[*]To whom correspondence should be addressed: Himangshu S. Bose, Ph.D.; Laboratory of Biochemistry, Biomedical Sciences, Mercer University School of Medicine and Memorial University Medical Center, Anderson Cancer Institute, 4700 Waters Avenue, Hoskins Research Building, Savannah, GA 31404, USA; Fax: (912) 350-1765; Email: bose_hs@mercer.edu

Keywords: 3β-hydroxysteroid dehydrogenase type 2 (3βHSD2), Translocase of Outer Mitochondrial Membrane 22 (Tom22), Steroidogenic Acute Regulatory protein (StAR), Pregnenolone, Progesterone, CHOP (C/EBP homology protein), Unfolded Protein Response (UPR), ER stress, Mitochondria.

ABSTRACT

The acute response to stress consists of a series of physiological programs to promote survival by generating glucocorticoids and activating stress-response genes that increase the synthesis of many chaperone proteins specific to individual organelles. In the endoplasmic reticulum (ER), short-term stress triggers activation of the unfolded protein response (UPR) module that either leads to neutralization of the initial stress or adaption to it; chronic stress favors cell death. UPR induces expression of the transcription factor, C/EBP homology protein (CHOP), and its deletion protects against the lethal consequences of prolonged UPR. Here, we show that stress-induced CHOP expression coincides with increased metabolic activity. During stress, the ER and mitochondria comes close to each other, resulting in the formation of a complex consisting of the mitochondrial translocase, translocase of outer mitochondrial membrane 22 (Tom22), steroidogenic acute regulatory protein (StAR) and 3β-hydroxysteroid dehydrogenase type 2 (3βHSD2) via its intermembrane space (IMS)-exposed charged unstructured loop region. Stress increased the circulation of phosphates, which elevated pregnenolone synthesis by 2-fold by increasing the stability of 3βHSD2 and its association with the mitochondrial-associated ER membrane (MAM) and mitochondrial proteins. In summary, cytoplasmic CHOP plays a central role in coordinating the interaction of MAM proteins with the OMM translocase, Tom22, to activate metabolic activity in the IMS by enhanced phosphate circulation.

INTRODUCTION

The acute response to stress consists of a relatively stereotyped series of physiological programs to promote survival. It is mediated by the hypothalamic-pituitary-adrenal (HPA) axis, resulting in hypothalamic corticotropin releasing hormone (CRH) secretion that stimulates release of adrenocorticotropic hormone (ACTH) by the pituitary and subsequent adrenal glucocorticoid release. Stress signaling is a critical factor regulating major morphological changes in cells that may be dependent on the activation of Ca^{2+}-dependent protein kinase C (PKC) (1, 2). Mitochondrial stress may also induce retrograde signaling in mammalian cells (3). In an animal model of acute stress in which mice were exposed to temperature changes, improved physiological recovery, reduced mortality and hormonal changes were observed. Such stress also leads to transcriptional activation of genes that harbor stress response elements within their promoters. For example, heat shock elements (HSEs) are found in the promoters of genes encoding proteins representative of all subcellular compartments (4), enabling cells to respond to global stress by increased synthesis of heat shock proteins and other molecular chaperones (5). Cells can also respond to stress in a way that is specific to individual organelles. Specifically, the endoplasmic reticulum (ER) stress response or the unfolded protein response (UPR) is activated in response to mild or short-term stress triggers, inducing the expression of a wide range of genes involved in the maintenance of ER function (6). In contrast, severe or long-lasting stress favors activation of a proapoptotic module that will lead to cell death.

Abnormal protein conformation disturbs cellular homeostasis and is considered a cause of many diseases, including developmental abnormalities. Signal transduction cascades are activated to restore the ER to its normal physiological state. The most abundant ER chaperone, the 78-kilodalton glucose-regulated protein (GRP78/BiP), is responsible for maintaining the permeability barrier of the ER during protein translocation, guiding protein folding and assembly, and targeting misfolded proteins for degradation (7). In unstressed cells, a fraction of ER-luminal GRP78 is bound to three different ER transmembrane proteins: (i) inositol-requiring kinase/endoribonuclease 1 (IRE1), (ii) a protein kinase activated by double-stranded RNA, (PKR)-like ER kinase (PERK), and (iii) activating transcription factor 6 (ATF6) (7). Binding of GRP78 to the ER-luminal domains of these proteins maintains them in an inactive state. Upon ER stress and concomitant accumulation of

misfolded and unprocessed proteins, GRP78 is sequestered away from PERK, IRE1, and ATF6 in order to attend to the increased need for protein folding (7).

The CHOP gene encoding the bZIP transcription factor, CHOP [C/EBP homology protein, also called GADD 153], is unregulated by JNK2 kinase and activator protein-1 (AP-1) (8) in response to the UPR (9). Studies using CHOP-null mice have established its role in ER-stress-induced apoptosis; CHOP deletion protects against the lethal consequences of prolonged UPR (10). Because both cells and animals lacking CHOP are protected against different physiological problems, CHOP may have a role in different cellular functions, possibly impacting both viability and apoptosis (11). However, it is not clear whether CHOP is directly inducing apoptosis or whether cell dysfunction and death arise as a secondary consequence of CHOP activity. CHOP likely has a protective role in maintaining ER function, and CHOP expression in response to stress impacts mitochondrial biogenesis through its chaperone activity (10).

Impaired stress response arises from either primary defects in the adrenal gland or secondary hypothalamic or pituitary defects, resulting in steroidogenesis defects. Mitochondrial proteins, enzymes and translocases responsible for steroid synthesis are encoded by the nucleus, synthesized in cytosol, and then targeted to mitochondria (Fig. 1A) (12-15). Outer and inner mitochondrial membrane (OMM and IMM, respectively) translocator protein assemblies, including TOM (Translocase, Outer Membrane) and TIM (Translocase, Inner Membrane), translocate and sort proteins into mitochondria. For example, on acute stress or hormonal stimulation, steroidogenic acute regulatory protein (StAR) is synthesized in the cytoplasm. It first interacts with the OMM-associated voltage-dependent anion channel 2 (VDAC2) followed by VDAC1, which is necessary for it to achieve an active conformation to foster cholesterol from the OMM to the IMM (16). Next, 3-beta-hydroxysteroid dehydrogenase type-2 (3βHSD2), which catalyzes pregnenolone to progesterone and DHEA to androstenedione conversion, interacts with the IMM translocase, Tim50, from the C-terminal to the inter membrane space (IMS) (17, 18). Given the interaction of Tim50 and Tim23 in the IMS, it was not surprisingly that 3βHSD2 also formed a transient association with Tim23 and regions of Tom22, generating a larger complex (Fig. 1B) (17). Tom22, an OMM-associated protein facing the cytoplasm, acts as a receptor for protein sorting and translocation of OMM proteins targeted to mitochondria (19). Knockdown of Tim50 expression reduced the expression of 3βHSD2 by 80% as well as decreased its activity (17). Moreover, knockdown of

either Tim23 or Tom22 reduced the conversion of DHEA to androstenedione by 3βHSD2 without affecting P450c17 (17), supporting the notion that 3βHSD2 requires mitochondrial translocases for steroidogenic and metabolic activity. Using an *in vivo* mouse model of stress, we found that the ER and mitochondria come in close proximity to each other, resulting in a complex containing mitochondrial StAR, Tom22 and 3βHSD2 (Fig. 1B).

Given its role in stress, we hypothesized that acute stress-induced CHOP expression may increase StAR protein levels and facilitate cholesterol transport (Fig. 1B), resulting in increased pregnenolone synthesis. In this article, we provide the first direct evidence of how adrenal steroid production is preferentially induced by CHOP expression without affecting other mitochondrial or ER proteins. Specifically, CHOP facilitates a supply of phosphates into the mitochondria, resulting in increased steroid synthesis by stabilizing 3βHSD2 protein conformation and its association with neighboring proteins.

MATERIALS AND METHODS

Cell culture, generation of CHOP knockdown cells (ΔCHOP cells) and Construction of plasmids

The mouse Leydig tumor cell line (MA-10) was grown in Waymouth media containing 15% horse serum, 5% fetal bovine serum and 1× Gentamycin. Cells were maintained at 37˚C in a humidified incubator under 5% CO_2. The pSilencer siRNA expression plasmid for CHOP was obtained from Open Biosystems (20). For generation of stable ΔCHOP MA-10 cells, the cells were transfected with the purified plasmid using Oligofectamine (Invitrogen, Carlsbad, CA, USA), and single clones were generated 48 h after transfection by limiting dilution into a selection medium containing 600 mg/mL of G418 (Geneticin; Life Technology, CA). Individual clones were then transferred to 24-well plates for propagation and then later transferred to 6-cm plates for transfection. Individual clones were examined for CHOP expression by Western blotting.

Construction of the full-length Tom22 and 3βHSD2 or different mutants cDNA expression cDNA vectors was described before (16). The accuracy of all clones was confirmed by sequencing in both direction through a commercial resource (MC Cloning lab, South San Francisco, CA). siRNAs for Tom22 were obtained from Life Technologies. COS-1 or MA-10 cells were transfected with 30 pmol siRNA (17), respectively, using oligofectamine (Life Technology, CA). Non-targeting siRNA as well as a combination of two non-targeting scrambled siRNAs (Life Technology) were included as controls in all experiments. In a specific experiment, we

also incubated with 100 ng/ml Trilostane (Gift from Dr. Gavin Vinson, University of London) as an inhibitor for 3βHSD2. The accuracy of the knockdown was determined by Western blotting.

Animal model

Male wild-type (WT) and CHOP-null mice were purchased from Jackson Laboratories (Bar Harbor Maine, USA). All mice were maintained in a pathogen-free facility and placed on a standard chow diet (AIN93G, Harlan Teklad Global Diets) for 4 weeks. The experimental procedure was approved by the Institutional Animal Care and Use Committee (IACUC number# A1406011 on September 8, 2014). To induce acute stress, animals were randomly divided into two groups: (i) control animals exposed ambient air at room temperature and (ii) experimental animals exposed to 10˚C for 1h in each day for 14 days. There were six animals in each group and each experiment was repeated three times independently. All animals were sacrificed immediately after their experimental procedure at day 14. Blood samples were collected through a heart puncture at the time they were sacrificed, and the adrenal and testicular tissues were excised, rinsed in ice-cold buffer, and processed for metabolic conversion immediately.

Isolation, purification and fractionation of mitochondria

Mitochondria were isolated from cells or mouse adrenal tissues. For mitochondrial isolation, adrenal tissues were diced in mitochondrial isolation buffer (250 mM sucrose, 10 mM HEPES, 1 mM EGTA, pH 7.4); MA-10 or COS-1 cells were washed with PBS two times and then isolated mitochondria following our previously developed procedure (17, 21). For most of the experiments, fresh mitochondria were used immediately after their isolation from tissues or cells.

The mitochondrial compartments were individually purified following a standard procedure with minor modifications (22). In brief, the OMM fraction was extracted with 1.2% digitonin, and the remaining mixture of matrix and IMM was purified through 0.5% Lubrol, where the matrix fraction remained in solution after centrifugation, and the IMM fraction formed the pellet. The purity of mitochondrial fractions was confirmed by assessing the levels of compartment-specific proteins.

Native polyacrylamide gel electrophoresis (PAGE)

To analyze complex formation, mitochondria were isolated from MA-10 cells and ΔCHOP MA-10 cells. The native complex was isolated by incubating the isolated mitochondria with buffer containing 1%

digitonin, and samples were separated by electrophoresis through 3-16% gradient native gels. Next, the protein complexes were transferred to a membrane and then probed with antibodies against 3βHSD2 and CHOP.

3βHSD2 protein purification and Conformational analysis

3βHSD2 was expressed as a recombinant protein in the baculovirus system (23). The concentrations of the unfolded proteins were determined with guanidinium hydrochloride to avoid errors in extinction coefficients (24). Multiple scans were averaged to improve the signal-to-noise ratio. Appropriate buffer baselines were obtained under the same experimental conditions and were subtracted from the sample spectra. Far-UV (195-250 nm) circular dichroism (CD) measurements were carried out in a Jasco spectropolarimeter (JASCO -815, Japan) at 20˚C with a 1.0-mm path length cuvette containing 175 mg/mL (1.52×10^{-6} M) protein in 10 mM NaH_2PO_4, pH 7.5. Spectra shown are the averages of three consecutive scans that were performed at a scan speed of 20 nm/min and corrected by subtracting corresponding blanks. Results are presented as mean residue molar ellipticity (Θ): $[\Theta]_r = \theta_{obs} / (10nlc)$, where θ_{obs} is the measured ellipticity in millidegrees, 'n' the number of residues in the protein, 'l' the path length of the cell expressed in cm, and 'c' the molar concentration of protein. Thermal melting (Tm) studies were performed in temperatures ranging from 4°C to 80°C, and the data was collected at 208 nm and 222 nm with a 0.2°C/min rate. For protein stabilization studies, the Tm of 3βHSD2 with and without shrimp alkaline phosphatase (SAP) treatment was performed with 10 mM NaH_2PO_4 and 10 mM $C_2H_3NaO_2$.

Proteolytic digestion experiments

Proteolytic digestion experiments were performed at 4°C or room temperature using various concentrations of proteinase K (PK; Sigma, St. Louis, MO). The limited digestion experiments were performed using 12.5 µg of total protein and different concentrations of PK for either 15 or 45 min. The reactions were terminated by the addition of an equal volume of SDS sample buffer containing 2 mM PMSF and then incubating in a boiling water bath. After electrophoresis, the samples were processed for Western blotting using the indicated antibodies.

Western blot analysis

Protein (12.5 µg) was separated by 15% SDS-PAGE and transferred to a polyvinylidine difluoride (PVDF) membrane (Millipore, Billerica, MA, USA). The membrane was blocked with 3% nonfat dry milk for

45 min, probed overnight with the primary antibodies, and then incubated with the peroxide-conjugated goat anti-rabbit IgG or anti mouse IgG (Pierce). Signals were developed with a chemiluminescent reagent (Pierce).

Mitochondrial viability assay

To check the mitochondrial activity and its membrane responsiveness, ATP assays were performed using an ATP Assay System Bioluminescence Detection Kit (ENLITEN, Promega, Madison, WI, USA) with a luminometer (Veritas microplate luminometer, Turner Biosystems) following the manufacturer's protocol. Basic mitochondrial activity was determined in terms of ATP production, and mitochondrial activity was inhibited by incubation of MA-10 cells and ΔCHOP mitochondria with various concentrations of mCCP (Carbonyl cyanide m-chlorophenyl hydrazone) for 1h.

Metabolic conversion assays

Isolated mitochondria from murine adrenals or steroidogenic MA-10 cells (300 µg) were incubated in phosphate buffer for metabolic conversion experiments. For the ^{3}H-pregnenolone to progesterone assay, 3x10^{6} counts of ^{3}H-pregnenolone were used for each reaction, which was chased with 30 µg of cold unlabeled progesterone (25). The metabolic reaction was initiated by addition of NAD and incubated at 37°C with continuous shaking for 4 h. In the case of ^{14}C-cholesterol to pregnenolone, 80,000 counts of ^{14}C-cholesterol were used for each reaction and chased with 20 µg of unlabeled cholesterol. For metabolic conversion of cholesterol to pregnenolone, the reaction was initiated by addition of NADPH and the reaction mixture was incubated at 37°C with continuous shaking for 3 h. To ensure complete conversion, we used 5-fold excess cold carrier in order to reach the saturation point. The steroids were extracted with ether/acetone (9:1 v/v), and equal amounts of a cold pregnenolone-progesterone mixture (for pregnenolone-progesterone assay) and cold cholesterol-pregnenolone mixture (for ^{14}C-cholesterol to pregnenolone) in CH_2Cl_2 was added as a carrier. The extracts were concentrated under a stream of nitrogen and then separated by TLC (Whatman, Sigma, St. Louis, MO) using a chloroform/ethyl acetate (3:1) mobile phase.

Gas chromatography-mass spectrometry (GC-MS)

The spots extracted from TLC plates were subjected to GC-MS analysis (Agilent 7890 GC and 5975C mass spectrometer). The column was an Agilent HP-5 with dimensions of 30 µM × 0.25 µm inner diameter with a 0.25 µm film thickness. Samples were dissolved in 50 µL of CH_2Cl_2, and 1 µL was injected onto the

column using a pulsed splitless injection. Helium was used as the carrier gas at a flow rate of 1 mL/min. The temperature program is as follows: ramp at 10°C/min from 70° to 310°C and hold for 6 min. Spectra were collected in full scan with 70 Ev ionization mode over the mass range of m/z 50 to 500 to facilitate comparison of MS spectra.

Co-immunoprecipitation (co-IP) analysis

Specific antibodies were pre-incubated with protein A-Sepharose CL 4B (0.5 µg/µL, Amersham Biosciences, Sweden) in 100 µL of 1× co-IP buffer (1% Triton X-100, 200 mM NaCl and 0.5% sodium deoxycholate) and mixed on an end-over-end rotator for 2 h at 4°C. To remove unbound antibody, the beads were washed with 1× co-IP buffer five times and then incubated again with rabbit IgG control antibody (Sigma) for 1 h to block unbound beads. After another series of washes to remove unbound antibody, the freshly isolated mitochondrial pellet (25 mg for each sample) was resuspended with ice cold lysis buffer (20 mM Tris HCl, pH 8.0, 137 mM NaCl, 10% glycerol, 1% Triton X-100, 2 mM EDTA) and incubated at 4°C for 15 min. Insoluble material was removed by ultracentrifugation (30 min at 100,000 ×g). The supernatants were incubated overnight at 4°C with end-over-end shaking in the presence of antibodies prebound to protein A Sepharose beads. After five to six washes with 1× co-IP buffer and two washes with 10 mM HEPES (pH 7.4), the protein A-Sepharose pellets were resuspended and vortexed with 100 mM Glycine (pH 3.0) for 10 sec. The sample pH was changed to pH 7.4 by adding a pre-titrated volume of 1.0 M Tris (pH 9.5), and the beads were separated from the soluble material by centrifugation at 2000 ×g for 2 min. The supernatants (immune complexes) were analyzed by Western blotting.

The dephosphorylation studies were performed with 10 mM Tris (pH 7.4), where purified mitochondria were washed with 10 mM Tris (pH 7.4) prior to the metabolic conversion assay. 3βHSD2 and mitochondria were phosphate deprived individually by incubating each with 10 mM Tris (pH 7.4) for 1 h at 37°C after which activity was determined. For rephosphorylation studies, various concentrations of 1 mM NaH_2PO_4 (pH 7.4) was added back to phosphate-devoid samples following the removal of the electrolytes through dialysis.

Histological analysis

Adrenal glands were fixed in zinc formalin, processed, and embedded in paraffin for routine light microscopy. Sections of 5-10 µm were obtained from each specimen, floated onto glass slides, stained with

hematoxylin and eosin (H&E), and examined by microscopy. For immunohistochemistry analysis, additional slides from each specimen were deparaffinized, rehydrated, and stained with either polycloncal antisera (dilution 1:100) or the monoclonal antibodies of the following dilutions: neat, 1:20, 1:50, and 1:100. Binding of the primary antiserum was detected by using the appropriate biotinylated secondary immunoglobulin followed by an avidin-peroxidase conjugate with diaminobenzidene as the chromogen. Negative control sections were treated in identical fashion except for the substitution of nonimmune goat serum for primary antisera or antibody. Sections were counterstained with hematoxylin.

Measurement of serum corticosterone

After completion of stress experiment blood was collected immediately from the experimental animals in an eppendorf tube through cardiac puncture and incubated at room temperature for 30 minutes. The serum was collected by centrifugation at 3000Xg for 10 minutes. To determine corticosterone concentration the serum was further diluted at various concentrations to a final volume of 50 microliter and the corticosterone was measured by radioimmunoassay (RIA) following manufacturer's protocol (Corticosterone ^{3}H RIA kit; MP Biomedicals, CA). The radioactivity was measured in a Scintillation counter (Beckman, CA).

Measurement of serum phosphate

To determine phosphate concentration 1, 2, 5, 10 and 50 microliter of serum was diluted to a final volume of 200 microliter and the phosphate concentration was determined by using Phosphate Assay Kit following manufacturer's protocol (Abcam, CA). The color development was detected in a luminometer (BioTek Synergy HT, CA) at 650 nm and the concentration was determined through an internal standard.

Computational modeling of 3βHSD2

Amino acid and nucleotide sequences were retrieved from the Swiss Protein Database (26). Next we performed the modeling using the Pymol Molecular Graphics system (Version 1.3 Schrodinger, LLC) (27) as described before (28).

Electron microscopy (EM)

To analyze the subcellular localization of 3βHSD2 and Tom22 in the mitochondria of both the steroidogenic MA-10 cells, EM experiments were performed. The cells (6×10^{6} MA-10 cells) were washed twice with PBS, gently scraped in the presence of PBS and transferred to 50 mL plastic disposable Corning

tubes. After centrifugation at 1470xg (Beckman Allegra 22R and rotor F630) for 10 min, the cells were fixed in 4% formaldehyde and 0.2% glutaraldehyde in 0.1M sodium cacodylate buffer, pH 7.4, dehydrated with a graded ethanol series through 95% and embedded in LR white resin. Thin sections of 75 nm thickness were cut with a diamond knife on a Leica EM UC6 ultramicrotome (Leica Microsystems, Bannockburn, IL) and collected on 200 mesh nickel grids. The sections were first blocked in 0.1% BSA in PBS for 4 h at room temperature in a humidified atmosphere followed by incubation with a 1:50 dilution of Tom22 antibodies in 0.1% BSA overnight at 4°C. The sections were washed five times with PBS and floated on drops of anti-primary specific ultra small (<1.0 nm) Nanogold^{TM} reagent (Nanoprobes, Yaphank, NY, USA) diluted 1:2000 in 0.1% BSA in PBS for 2-4 h at room temperature. After fives washes with PBS and five with deionized H_2O, the sections were incubated with HQ Silver^{TM} (Nanoprobes) for 8 min for silver enhancement, followed by washing in deionized H_2O.

For double immunolabeling, the same sections were first labeled with a Tom22 antibody (1:2000) overnight at 4°C followed by incubation with 3βHSD2 antibody (1:2000) overnight at 4°C. Because the silver enhancement of the gold particles labeling Tom22 occurred for twice as long as the gold particles labeling 3βHSD2, it, therefore, produced two different sizes of gold particles. After a final wash, the grids were stained with 2% uranyl acetate in 70% ethanol to increase the contrast. The grids were washed five times with deionized H_2O and air dried. The large gold particles were an average of 55 nm in diameter with 90% of the gold particles being between 45-65 nm in diameter. The small gold particles were an average size of 15 nm with 90% of the gold particles being smaller than 25 nm in diameter. The cells were observed using a JEM 1230 transmission electron microscope (JEOL USA Inc., Peabody, MA, USA) at 110 kV and imaged with an UltraScan 4000 CCD camera and First Light Digital Camera Controller (Gatan Inc., Pleasanton, CA, USA). Forty sections from each experiment were analyzed.

Computational modeling of Tom22

We developed a 3D structural model of Tom22 (NCBI NP_064628.1, Uniprot Q9NS69) sequence (AA 1-142) using the structures of NAD-dependent aldehyde dehydrogenase from *Lactobacillus acidophilus* (3ROS) and Esta from *Arthrobacter nitroguajacolicus* (3ZYT) as templates using the programs YASARA (29) and WHATIF (30). First, we performed a PhiBlast search of the PDB database with the amino acid sequence of

Tom22 to create a custom position-specific scoring matrix (PSSM) that was then used in further runs of PhiBlast searches to identify structurally similar sequences. A secondary structure prediction of the sequence was used to perform the structure-based alignment of the sequences using the PSI-Pred secondary structure algorithm (31). Aligned sequences were subsequently analyzed by YASARA and WHATIF. Some of the loops were modelled separately by scanning a library of loop databases that predicted that Tom22 should have a minimum amino acid region facing the IMS. Side chains were optimized by molecular dynamic (MD) simulations. The final model was refined by a 500 ps (MD) simulation using AMBER 2003 force field and checked with WHATCHECK (32), WHATIF (30), Verify3D (33, 34) and Ramachandran plot analysis (35, 36). Structures were depicted with Pymol (www.pymol.org) and rendered as ray-traced images with POV-RAY (www.povray.org). The MD simulations were performed using the AMBER03 force field (29). The simulation cell was filled with water, the pH was fixed to 7.4, and the AMBER03 (37) electrostatic potentials were evaluated for water molecules in the simulation cell and adjusted by addition of sodium and chloride ions. The final MD simulations were then run with AMBER03 force field at 298K, 0.9% NaCl and pH 7.4 for 500 ps to refine the models. The best models were selected for analysis and evaluation.

Figure preparation and statistical data analysis

The images were obtained from the autoradiogram or scanning through a phosphorimager and the data analysis was performed using Origin software (OriginLab Corporation, Northampton, MA) or Microsoft Excel. The mean of the data was compared between different animal groups and p-value was significantly concerned at 0.05 levels. The data analysis was performed by hypothesis testing for quantifying group comparisons. The parameters were compared between two specific groups and *p*-value was determined by Student's *t*-test.

RESULTS

Acute stress increases adrenal steroidogenesis in vivo

Within the lumen of the ER, protein chaperones assist in folding newly synthesized polypeptides and preventing aggregation of unfolded or misfolded proteins (38). The most abundant ER chaperone, GRP78, is responsible for maintaining the permeability barrier of the ER during protein translocation, and associates with the transmembrane ER stress sensors, IRE1-1 and ATF6 (Fig. 1B). Thus, we determined the impact of ER stress on the expression of ER- and mitochondrial-associated ER membrane (MAM)-resident proteins and

identified an effect on mitochondrial metabolic activity. Specifically, ER stress induced by a change in temperature for 1 h/day for 14 continuous days did not alter GRP78, Calnexin, COX-IV, VDAC2, HSP70, or 3βHSD2 protein expression (Fig. 1C). However, the expression of StAR was marginally induced, and CHOP protein was highly induced with exposure to stress (Fig. 1C).

To understand the effect of increased CHOP expression on mitochondrial activity, we next determined pregnenolone and progesterone synthesis in response to stress. As shown in Fig. 1D (top left panel), pregnenolone synthesis increased in response to stress from 15 ng/mL to 32 ng/mL (right panel). Because StAR expression was only moderately increased with stress, the increased metabolic activity is likely due to the appearance of CHOP, which may increase StAR activity by altering its folding to facilitate more cholesterol transfer.

To understand the effect of stress on progesterone synthesis, we performed metabolic conversion assays to evaluate pregnenolone to progesterone conversion. As shown in Fig. 1E, progesterone synthesis increased in response to stress from 18 ng/mL to 37 ng/mL. Western blot analysis of the mitochondria applied in each reaction from both Fig. 1D and 1E (bottom panels) shows that 3βHSD2 and VDAC2 levels were similar. Measurement of stress by serum corticosterone analysis showed an increase from 1.4 ng/ml to 1.68 ng/ml ($p \leq 0.0003$) after stress (Fig. 1F). Thus, stress increased the availability of the substrate, pregnenolone (Fig. 1D), by two-fold, in the absence of large changes in protein expression. Because protein folding is a rapid process, stress may have induced changes in 3βHSD2 folding, which may be mediated by CHOP.

Cytoplasmic CHOP interacts with MAM-associated StAR

To determine the role of CHOP in folding IMS-resident proteins, we established stable MA-10 cells expressing CHOP siRNA (ΔCHOP MA-10 cells). As shown in Fig. 2A, CHOP expression was undetectable following its silencing (left panel). We next isolated the crude mitochondria, which also includes proteins from the MAM (39), from the WT and ΔCHOP MA-10 cells, solubilized with digitonin, separated the protein complexes via native-gradient PAGE, and stained with a 3βHSD2 antibody (Fig. 2A, right panel). Two complexes of 750 and approximately 550 kDa were identified; however, the intensity of the complexes was lower in the ΔCHOP MA-10 cells, which may be due to the reduced concentration of the active 3βHSD2 and StAR in the absence of CHOP expression.

To identify the proteins present within the two complexes, we performed mass spectrometry (LC MS/MS) analysis. As shown in Tables 1 and 2, the proteins present in both the complexes from the WT cells, including MAM- and OMM-resident proteins, were similar, suggesting that the 550 kDa complex (Table 2) is possibly a breakdown of the larger 750 kDa complex (Table 1). Only Tom22 disappeared from the 3βHSD2-containing complex in the absence of CHOP (Tables 3 and 4), suggesting that it may bridge the OMM side facing the cytoplasm and the IMS of the mitochondria. The absence of Tom22 in the 3βHSD2-containing complex in ΔCHOP cells suggests that its signal is either below the level of detection of the system or that it is buried within the sequence, where stress facilitates the interaction of Tom22 with other mitochondrial proteins, as well as the proteins present at the MAM.

To understand the impact of stress and, therefore, CHOP expression on 3βHSD2 and Tom22 interaction, we performed co-IP analysis with adrenal mitochondrial fractions. Under unstressed conditions, 3βHSD2 interacts with StAR, VDAC2, but not with Tom22 (Fig. 2B, top panel). However, Tom22 antibody recognized 3βHSD2 minimally showing a partial interaction between Tom22 and 3βHSD2 possibly due to the availability of all the Tom22 epitopes (Fig. 2B, Tom22 panel). In the absence of stress, CHOP is not expressed and, thus, did not interact with 3βHSD2 or VDAC2 (Fig. 2B, bottom Panel). However, in the presence of stress, the interaction between 3βHSD2 and StAR was increased, and interaction between 3βHSD2 and Tom22 was observed (Fig. 2C, top panel). As expected, CHOP expression was induced (Fig. 2C, bottom panel). In the CHOP-null mice after stress, no interaction was noticed between StAR and Tom22 (Fig. 2D, second panel from the top) or between 3βHSD2 and Tom22 (Fig. 2D, top panel). For further confirmation about the roles of CHOP and VDAC2, we analyzed protein expression in MA-10 and COS-1 cells along with adrenal lysates from mice with or without stress. In CHOP knockdown mice adrenals, StAR expression was similar to the level observed in WT mice (StAR lane), and the expression of mitochondrial 3βHSD2, GRP78, and calnexin remained unchanged (Fig. 2E). As expected nonsteroidogenic COS-1 cells only expressed VDAC2, GRP78, calnexin and HSP70, but not StAR and 3βHSD2 (Fig. 2E). We have also examined mitochondrial viability by measuring the ATP release before and after addition of increasing amounts of mCCP to the mitochondria isolated from WT and ΔCHOP MA-10 cells. As shown in Fig. 2F, no difference in mitochondrial ATP content was detected between the two cell lines. Thus, CHOP may facilitate the interaction between StAR and 3βHSD2

or Tom22. Given that the majority of CHOP is found within the ER and MAM (Fig. 2G, top panel), its interaction with 3βHSD2 may be facilitated by Tom22.

Domains mediating StAR-Tom22 interaction

Tom22 is an OMM-associated mitochondrial receptor that interacts with IMM-associated 3βHSD2 via its C-terminus that is exposed to the IMS (17). We hypothesized that CHOP might directly influence Tom22 activity or alternatively work in conjunction with StAR. Because the complete 3-dimesional (3D) structure of Tom22 is unknown, we developed a 3D structural model of the Tom22 (NCBI NP_064628.1, Uniprot Q9NS69) sequence (AA 1-142) using the structures of NAD-dependent aldehyde dehydrogenase from *L. acidophilus* (3ROS) and Esta from *A. nitroguajacolicus* (3ZYT) as templates and YASARA (29). As shown in Fig. 2H and J, the Tom22 structural model indicates that it should have a minimum amino acid region facing the IMS. A space filling model integrated with the membrane (Fig. 2I) indicates that the L2 loop is out of the membrane facing the cytoplasm. Similarly only a small, unstructured stretch of 20 amino acids from the C-terminus is exposed to the IMS. Thus, it is likely that the L2 loop comprising the acidic amino acids "EEDDDEELD" might be responsible for interaction with proteins from the cytoplasm, including StAR. However, the complete unstructured L8 loop in combination with the H8 helix might be responsible for interaction with 3βHSD2. Furthermore, the basic amino acids within the smaller transmembrane loop L6 may participate in interaction; however, its short length makes this less likely because of the cost of entropy required for opening will be higher than the energetic stabilization forming complex. Taken together, the loose regions of Tom22 (Fig. 2H) facing the IMS are likely critical for its interaction with 3βHSD2, which has a flexible conformation.

To identify specific amino acids required for Tom22-3βHSD2 interaction we expressed Tom22 mutants, in which an L2 aspartic acid (amino acids 35 and 37) or glutamic acid (amino acid 39) is changed to an alanine, in ΔTom22 MA-10 cells. As shown in Fig. 3A (top panel), Tom22 siRNA reduced Tom22 expression by >90%, and expression of WT, D35A and D37S amino acids restored Tom22 expression to levels similar to untreated MA-10 cells. The E39A and Δ35-39 Tom22 restored about 50% expression. VDAC2 expression remained unchanged (Fig. 3A, bottom panel). Mitochondrial compartmental fractionation (Fig. 3B) confirmed that the Tom22 proteins were localized at the OMM (Fig. 3B top panel) similar to the OMM marker, VDAC2 (Fig. 3B,

middle panel). To confirm that the mutants were integrated with the OMM in MA-10 cells after knockdown with siRNA of Tom22, we isolated mitochondrial compartments, and then immunoblotted with a Tom22 antibody. In addition to WT Tom22, the mutants, D35A, D37A, E39A and the three amino acid substituted mutant Tom22 (35-39 Mut), were present only with the OMM fraction similar to that observed for VDAC2 (Fig. 3C, top and second panels). The accuracy of mitochondrial fractionation was confirmed by staining the same fractions with the mitochondrial matrix protein, COX-IV, the OMM-associated VDAC2, the IMS resident protein 3βHSD2 and the IMM-associated Tim23 (40).

We next confirmed the localization of WT and mutant Tom22 through immune electron microscopy staining with Tom22 and 3βHSD2 antibodies independently and also together. WT Tom22 was present at the OMM (Fig. 3D, left bottom panels, red arrow). Co-staining for the IMS resident, 3βHSD2, confirmed that Tom22 (red arrows) was present at the OMM while 3βHSD2 (blue arrows) was localized inside the mitochondria (Fig 3D, right panels). The bottom panels show an enlarged view of mitochondrion presented above. Similar analyses with the Tom22 mutants revealed that 3βHSD2 (blue arrows) was present inside the mitochondria while the Tom22 mutants (red arrows) were at the OMM (Fig. 3E). In summary, within the L2 loop region facing the cytoplasm whether it is a point mutant or substitution of four amino acids still Tom22 folding remained unchanged.

Analysis of metabolic conversion of pregnenolone to progesterone showed that it was greatly reduced upon Tom22 knockdown (from 16.5 to 5 ng/mL) (Fig. 3F). Furthermore, expression of the D35A or E39A mutants did not restore metabolic activity as compared to the D37S mutant (Fig. 3F); the activity resulting following transfection with the triple mutant, D35A, D37S and E39A (35-39 Mut), was reduced by 90%. Overexpression of WT Tom22 restored metabolic activity by >80%. Similar results were observed when we analyzed the metabolic conversion of ^{14}C-cholesterol to ^{14}C-pregnenolone (Fig. 3G). In summary, the L2 loop region of Tom22 may play a significant role in regulating metabolic activity.

3βHSD2 is a loosely folded protein, and it is likely to interact with the loosely binding regions of Tom22. We next analyzed the interaction of the Tom22 mutants with 3βHSD2 by co-IP analysis. As shown in Fig. 3H, the intensity of the interaction decreased with the triple mutant almost completely, and also minimal interaction

with the D35A mutant was observed (Fig. 3H, middle panel). Wild-type cells do not express CHOP, which possibly assists in the interaction from the cytoplasmic side upon expression. Alternatively, the change in L2 loop amino acids possibly altered Tom22 conformation, resulting in a misfolded protein and suggesting that this region is responsible for interaction with StAR directly or through CHOP.

Tom22 L8 –H8 is essential for metabolic regulation

Tom22 has many unstructured regions (41), which allows it to remain flexible while associated with the membrane. The partially developed 3D-solution structure predicted that Tom22 should have a minimum amino acid region facing the IMS, comprising amino acids 128 to 142 (41), that may mediate its interaction with 3βHSD2 at the IMS. Although a smaller transmembrane loop with basic amino acids may participate in the interaction, its short length makes this less likely. To confirm that indeed the C-terminus of Tom22 is responsible for its interaction with 3βHSD2, we expressed various Tom22 mutants from small to large amino acids or from polar to nonpolar or basic amino acids, generating Q118L, T125I, M131R, A134D and N124K Tom22, and expressed these mutants in ΔTom22 MA-10 cells. So we knocked down Tom22 expression by siRNA in MA-10 cells (Fig 4A). Western blot analysis confirmed the Tom22 mutant expression (Fig. 4A, top panel), and mitochondrial fractionation confirmed their localization to the OMM (Fig. 4B). Electron microscopy was next employed to determine Tom22 mutant localization as well as that of the IMS resident, 3βHSD2 (Fig. 4C). As expected, 3βHSD2 (blue arrows) was present inside mitochondria, and the Tom22 mutants (red arrows) were associated with OMM.

Although progesterone conversion was not restored with M131R expression, it was restored upon expression of all other Tom22 mutants, Q118L, T125I, N124K, and A134D (Fig. 4D). Although amino acids 125-142 are within the unstructured L8 loop, only the M131R mutant did not restore complete activity, suggesting that the loop region possibly has a specific conformation, which is altered when the hydrophobic methionine is replaced with a charged, bulky polar amino acid. Surprisingly, the helix region Q118L mutant restored activity, which may be due to the similar size of the amino acid or that the mutation did not affect the folding due to lipid integration (Fig. 4D). Co-IP analysis confirmed that 3βHSD2 interacted with the N124K and T125I mutants preferentially at a higher intensity than the M131R, A134D and Q118L mutants (Fig. 4E, top and middle panels), suggesting that the unstructured region of Tom22 interacts with 3βHSD2. Arginine is a

large amino acid with a long carbon chain. There is possibly a change in conformation from methionine to Arginine of M131R resulting in loss of activity. However, it is possible that the A134D mutant is present inside the loop and thus it is not easily accessible to 3βHSD2 exposed sites for interaction resulting no loss in activity. In summary, these results confirmed that metabolic activity is increased due to the presence of CHOP in the cytoplasm, which acted on the charged amino acids of L2 loop, and that L8 loop is responsible for interaction with 3βHSD2 at the IMS.

Metabolic activity is dependent on phosphate circulation

We next sought to identify the condition in which Tom22 facilitates metabolic activity at the IMS. We hypothesized that phosphate circulation across the OMM is essential for mammalian pregnenolone synthesis albeit through an unknown mechanism possibly increasing stability in the complex (42). 3βHSD2 expression is not changed in response to stress and requires a molten globule conformation in an acidic environment for activity, facilitated by the mitochondrial proton pump (23). The presence of CHOP increased pregnenolone synthesis more than 2-fold in comparison to the absence of stress (Fig. 1D); therefore, we hypothesized that the OMM receptor, Tom22, possibly facilitates interaction with 3βHSD2 while interacting with StAR-VDAC2, resulting in increased enzymatic activity at the IMS in the presence of circulating phosphates. CHOP is expressed during stress, and facilitates interaction with 3βHSD2 through the StAR-VDAC2-Tom22 complex (Fig. 2C) and, thus, possibly plays a central role in increasing the circulation of phosphates in association with Tom22. However, no changes in adrenal 3βHSD2, Tom22, and VDAC2 expression were detected in either WT or CHOP-null mice in response to stress (Fig. 2E). Thus, we first attempted to determine a change in cellular architecture by immunohistochemistry analysis of Tom22, StAR, 3βHSD2, Aldosterone Synthase (AS), and VDAC2 expression (Fig. 5A and B); however, no remarkable change was noticed. Furthermore, EM analysis following Tom22 and 3βHSD2 staining showed that the mitochondrial architecture was not altered (Fig. 5C).

Mitochondrial metabolic activity is related to the circulation of phosphates from the OMM to the IMM, as knocking down phosphate carrier protein (PCP) reduced phosphate circulation and pregnenolone synthesis (22). Analysis of serum phosphate levels showed that it increased from 6.2 to 7.4 mM in WT mice ($p \leq 00029$) in response to stress; however, the CHOP-null mice had no significant change ($p = 0.153$) in phosphate concentration with stress (Fig. 6A). These results prompted us to explore the possibility that phosphates

increase metabolic activity by association with neighboring proteins, forming a network from the MAM to mitochondria. As shown in Fig. 6B (middle panel), addition of 5 mM phosphate to mitochondria increased the progesterone synthesis from 4 ng/mL to 8.0 ng/mL, peaking at 20 ng/mL with 100 mM phosphates (Fig. 6B, top panel).

To determine whether the increased phosphate concentration facilitated 3βHSD2 association with the translocases and increased its activity, we examined the progesterone levels produced with dephosphorylated 3βHSD2 protein and mitochondria. In the absence of 3βHSD2, no progesterone was synthesized, confirming that the isolated mitochondria have minimal endogenous activity (Fig. 6C). Incubation of 3βHSD2 with the mitochondria in the absence of phosphate or with mitochondria devoid of phosphate resulted in 4.1 ng/mL progesterone synthesis as compared to the 18 ng/mL of progesterone produced with normal 3βHSD2 and mitochondria (Fig. 6C). Incubation of mitochondria and dephosphorylated-3βHSD2 with sodium phosphate restored about 50% activity (Fig. 6D, top and right panels), suggesting that 3βHSD2 requires phosphate ions for progesterone synthesis. An increase in activity with SAP more than 0.5 Unit/µl suggests a reversible phosphorylation (43). The SAP enzymatic reaction proceeds through a covalent phosphoseryl intermediate to produce inorganic phosphates or to transfer phosphoryl group to alcohols resulting more phosphate ions (44) . So, the activity did not increase beyond 50%, as the inorganic phosphates inhibits shrimp alkaline phosphatase at higher concentrations (43); thus, when we incubated the reaction with external inorganic phosphates, only 50% of 3βHSD2 activity was restored.

The predicted phosphorylation sites were determined by the NetPhos program (45). Based on the computer modeling (46) and phosphorylation prediction (45), serine residues 123 and 124 were most crucial for S-S bonds and S-T bonds (Fig. 6E). Three more amino acids, T288, S358 and S369, are also possibly phosphorylated as these residues are exposed to the outer surface of the helical structure (Fig. 6E). The best structure binding site for post-translational modification of arginine 183 is present in the groove. To determine the specificity, we mutated arginine 183 to glutamic acid and changed S123, S124, T288, S358 and S369 to alanine and threonine, and determined progesterone synthesis following our earlier procedure (22). As shown in Fig. 6F, WT 3βHSD2 synthesized 7.9 ng/mL of pregnenolone; the S123A and S124A mutants had no activity. The S358A mutant also reduced the activity, synthesizing 2-3 ng/mL of pregnenolone. This is also possible that

the reduction in activity is due to the change in amino acids. To our surprise, mutating the bulky arginine at position 183 to glutamine also ablated 3βHSD2 activity similarly to the S123A or S124A mutants. Western blot analysis of the transfected cells showed similar levels of mutant 3βHSD2 expression as compared to the WT protein (Fig. 6G, top panel); VDAC2 expression levels were also similar (Fig. 6G, bottom panel). To confirm whether the inactivity is due to conformational change and not on phosphorylation, we changed S123A to S123T and similarly S124A to S124T. Also to completely rule out any error we also developed a combined serine to threonine mutant together of the 123 and 124 residues. The activity from S123T and S124T combined mutation or individual mutation ablated activity completely, suggesting that the reduction in activity is possibly due to change in amino acids not likely due to phosphorylation (Fig. 6H). Western blot analysis of the transfected cells showed similar levels of mutant S123T and S124T 3βHSD2 expression as compared to the WT and the amount of protein content applied in each lane was also identical as observed by staining with VDAC2 antibody (Fig. 6I). In summary, our results confirm that the reduced activity observed in the other mutants was likely not due to reduced phosphorylation but due to a change in the amino acids.

3βHSD2 conformation is stabilized by the circulation of phosphates

To better understand the role of phosphate circulation on Tom22 and 3βHSD2 function, we isolated mitochondria from MA-10 cells, which were devoid of phosphate. After various concentrations of phosphates were added, the complexes were isolated, solubilized with digitonin, and analyzed by native gradient PAGE and staining with a 3βHSD2 antibody (Fig. 7A). The intensity of 450 kDa complex was increased more than 3.5 fold on addition of 5 mM phosphate to the phosphate deprived cells, but the intensity decreased dramatically with concentrations more than 15 mM (Fig. 7A and B). As a comparison, we isolated the mitochondria from MA-10 cells, then added various concentrations of phosphate and analyzed in an identical fashion as described above (Fig. 7C). The bottom panels show that the same amount of mitochondrial proteins was applied in each reaction (Fig. 7A and C). In the absence of phosphate, two complexes of 750 kDa and 450 kDa were observed (Fig. 7A). In the presence of low phosphate concentrations, the 450 kDa complex became more intense (Fig. 7C) with only the 750 kDa complex detected at high phosphate concentrations, suggesting that the addition of extra phosphate increased the stability of high molecular weight complex possibly through increased association of neighboring proteins. An analysis is presented in Figs. 7B and 7D.

We next determined how the phosphorylation of 3βHSD2 impacts its conformation by dephosphorylating active 3βHSD2 protein prepared by a baculovirus system and analyzing its conformation by CD. The equilibrium CD spectra of dephosphorylated and phosphorylated 3βHSD2 have minima at 208 and 222 nm, respectively, which is typical of a α-helical conformation (data not shown). We next determined the stability 3βHSD2 protein in presence and absence of phosphate by thermal denaturation to identify different states of the protein conformation. As shown in Fig. 7E, 3βHSD2 unfolds partially at 27˚C, after which it stabilizes until it starts unfolding at 41˚C and is completely unfolded at 59˚C with a Tm of 51˚C. The two-step unfolding is suggestive of complete denaturation (Fig. 7E), where the initial unfolding is possibly due to a cooperative intramolecular association with most of the domains and was resistant to unfolding because of its molten globule conformation (23). In the absence of phosphate anions, the protein displayed reduced stability, and the initial unfolding is lost. The initial Tm of the 3βHSD2 protein at 33˚C is suggestive of its retaining the initial change of one conformational state to the second one. This first unfolding is indicative of a pseudo-stable conformation in which most of the secondary structure is preserved and may serve as a way for the protein to maintain equilibrium with the native state.

At 33˚C, the enthalpy (ΔH) of 3βHSD2 was 1.2 kCal/mol, increasing to 4.1 kCal/mol at 50°C (Fig. 7E). When the salt concentration was increased to 1.0 M, the two-step unfolding was lost due to salt-induced denaturation (Fig. 7F). As seen from the model structure (Fig. 6E), the globular structure is extremely flexible. Thus, it is likely that the intramolecular association is favored by the phosphate anion on the positively charged amino acids, changing 3βHSD2 organization even at lower temperatures. In presence of phosphates, an equilibrium between the initial state of unfolding from $N \rightarrow I_u \Leftrightarrow Pu \geq IU(Tm) \rightarrow D$ to the unfolded state occurs through a three-step process (Fig. 7G). 3βHSD2 conformation from the initial unfolding state (Iu) to the pseudo-unfolded state (Pu) is in equilibrium at 33˚C. The protein undergoes an initial step of unfolding or an intermediate stage of unfolding (IU), which is the thermal unfolded state at 50˚C. In the next step, the protein undergoes complete unfolding or denaturation into an unfolded (D) state. In summary, the results strongly suggest that phosphate circulation increased 3βHSD2 association with neighboring proteins, resulting in increased stability and interaction with Tom22 and StAR.

DISCUSSION

Both the ER and mitochondria are dynamic organelles capable of modifying their structure and function in response to changing environmental conditions. ER and mitochondria interact both physiologically and functionally due to their close proximity (47). Newly synthesized proteins, including mitochondrial proteins, require folding within the ER lumen prior to trafficking to the next cellular compartment as programmed by their signal sequences. Specifically, nascent polypeptide chains emerge in the ER lumen, where posttranslational modifications, such as N-linked glycosylation and intra- and intermolecular disulfide bond formation, facilitate the folding of polypeptides to form specific tertiary and quaternary structures for proper protein function (48). The quality of protein folding is precisely monitored by an ER quality control system that only allows properly folded proteins to be transported to the specific organelle and directs misfolded proteins for ER-associated degradation (ERAD) by the 26S proteasome or for degradation through autophagy (49, 50). ER stress impairs this process and results in the accumulation of unfolded or misfolded proteins, resulting in UPR and the expression of a wide range of genes and activation of proteins involved in the maintenance of ER function (6), including IRE1, PERK, ATF6, and CHOP.

In the present study, CHOP expression did affect the expression of ER-, MAM-, or mitochondrial-resident proteins in the adrenal glands. The presence of CHOP at both the ER and MAM possibly influenced MAM and mitochondrial proteins. ER and mitochondria form close contacts with 20% of the mitochondrial surface in direct contact with the ER (51), which facilitates communication between the organelles (39). Thus, the purified MAM showed the presence of Tom22 and VDAC2, which are part of the MAM but permanently present at the mitochondria facing the OMM. Since Tom22 interacts with the IMS resident, 3βHSD2, it was pulled out during the co-IP analysis.

The expression of CHOP through stress coincided with increased mitochondrial metabolic activity. Because serum phosphate concentrations in CHOP-null mice exposed to stress were reduced by approximately 20% as compared to WT mice exposed to stress (Fig. 6A), we hypothesized that an increase in mitochondrial phosphate supply could stabilize 3βHSD2 conformation, increasing metabolic activity that resulted in >2-fold progesterone synthesis. The presence or absence of CHOP expression did not alter the expression of other ER-resident or mitochondrial proteins. Because CHOP is a chaperone, it may assist in the folding of Tom22 and

StAR, especially given that it was located both in the ER and MAM regions of adrenal cells. Tom22 is a MAM-associated protein from the mitochondrial side; however, CHOP faces the ER side of the MAM, suggesting that they only transiently interact, which may be why CHOP interaction with Tom22 was not demonstrated by co-IP analysis in the absence of stress (Fig. 2B, top panel). Similarly, StAR is synthesized on acute hormonal regulation or during stress, remaining at the MAM prior to loading onto the VDAC-containing region of the OMM. Tom22, VDAC2, and StAR are all part of a MAM fraction. There is a partial interaction between Tom22 and 3βHSD2 at the IMS, but interaction is stronger under stress condition. It is possible that stress generated changes in the conformation of StAR that were mediated by the chaperonic properties of CHOP.

Expression of Tom22 mutants did not fully restore the metabolic activity of ΔTom22 cells, suggesting that the mutants were possibly misfolded as their accurate localization was confirmed. Although Tom22 appears flexible, it may become significantly structured upon OMM integration, especially given that the mutation in the H8 helix did not ablate activity but a mutation in the unstructured loop region (L8) completely ablated activity. An L2 mutant also failed to interact with 3βHSD2 via co-IP analysis, suggesting that this region is crucial for metabolic regulation at the IMS. Since StAR residency is shorter at the MAM and longer at the OMM, stress may have facilitated a structural change in Tom22 due to the presence of flexible folding associated with the lipid membrane. As a result, the mitochondrial import channel may have opened, resulting in increased metabolic activity with the presence of more phosphates, while the substrate remained the same for the isomerase and dehydrogenase activities at the IMS (23).

Stress-induced CHOP expression coincided with a 2-fold increase in pregnenolone synthesis (Fig. 1D), which is possibly due to the 1.5-fold increase in expression of StAR (Fig. 1C). Through physical interaction, CHOP may have facilitated a conformational change in Tom22 or in StAR-Tom22. StAR is transiently associated at the MAM from the ER side, so it is more likely facilitated through StAR. Thus, CHOP may push Tom22 like a piston, resulting in the L8 loop of Tom22 coming in close proximity to 3βHSD2, facilitating its catalysis. This would explain how a mild increase in StAR expression by stress increased the catalytic reaction by two-fold largely independent of changing protein concentration.

The presence of increased phosphates stabilized 3βHSD2 protein conformation by increasing its interaction with neighboring proteins. The intensity of the 450 kDa 3βHSD2-containing complex increased following

addition of low concentrations of phosphate with higher phosphate concentrations stabilizing the 750 kDa complex alone (Fig. 7A), suggesting that the presence of phosphate increased association of Tom22 with the neighboring proteins from the OMM-exposed region. The association is possibly facilitated by the stabilization of 3βHSD2 conformation as confirmed by its higher Tm (Fig. 7E and F). Thus, the circulation of phosphates possibly facilitates the stabilization of 3βHSD2 in a dynamic state and may be mediated by the presence of CHOP interacting with Tom22 or StAR-Tom22.

The molecular identity of the mitochondrial permeability pore, which is comprised of dimers of the mitochondrial ATP synthase (52), is now better understood. IMM permeability is increased in response to stress, leading to the formation of the voltage-dependent nonspecific pore, PTP (53), that is permeable to water, ions, and substances of low molecular mass. Chronic stress leads to mitochondrial dysfunction due to extensive PTP opening and ATP hydrolysis, during which the cells cannot maintain structural and functional integrity. In addition, protein conformation cannot be restored under chronic stress. In the stress model used in the present study, acute stress likely restored PTP to its original conformation, increasing the phosphate concentration within the mitochondria due to PTP closure.

In summary, short periods of stress increased the metabolic activity of adrenal cells that coincided with increased CHOP expression. Either directly or through StAR, CHOP acts on the mitochondrial translocase, Tom22, facilitating its interaction with 3βHSD2 via its IMS-exposed unstructured region. Stress also facilitated phosphate transport into the mitochondria, which stabilized 3βHSD2 conformation likely via circulation of phosphates and increasing its activity.

ACKNOWLEDGEMENTS

HB was supported by grants from the National Institutes of Health (HD057876) and the Anderson Cancer Institute. We are thankful to Dr. Satyam Banerjee for participating during preliminary experiments and performing the animal surgeries. We are also thankful to Mr. Greg Roberson for the maintenance of animals and his assistance during the experimental procedures and John Knights for assistance in the immunohistochemistry image capturing. MP is thankful to Mr. Subodh Thapliyal for his help in statistical analysis.

Conflict of Interests: The authors declare that they have no conflict of interest.

635 **Authors Contribution:** HB conceptualized the project, analyzed the data and wrote the manuscript; MP,
636 WEB, JK, SAP, AW, AVP, GP and RMW performed the experiments; JLT provided reagents and MP prepared
637 all the figures and analysed data. A complete manuscript was available to all of the authors prior to initial
638 submission.
639

REFERENCES

1. **Amuthan G, Biswas G, Zhang S-Y, Klein-Szanto A, Vijayasarathy C, Avadhani NG.** 2001. Mitochondria-to nucleus stress signalling induces phenotypic changes, tumor progression and cell invasion. EMBO J **20:**1910-1920.
2. **Amuthan G, Biswas G, Anandaatheerthavarada HK, Vijayasarathy C, Shephard HM, Avadhani NG.** 2002. Mitochondrial stress-induced calcium signalling, phenotypic changes and invasive behavior in human lung carcinoma A549 cells. Oncogene **21:**7839-7849.
3. **Biswas G, Guha M, Avadhani NG.** 2005. Mitochondra-to nucleus stress signalling in mammalian cells: Nature of nuclear gene targets, transcription regulation, and induced resistance to apoptosis. Gene **354:**132-139.
4. **Morimoto RI.** 1998. Regulation of the heat shock transcriptional response: cross talk between a family of heat shock factors, molecular chaperones and negative regulators. Genes Dev **12:**3788-3796.
5. **Hartl FU.** 1996. Molecular chaperones n cellular protein folding. Nature **381:**571-579.
6. **Travers KJ, Patil CK, Wodicka L, Lockhart DJ, Weissman JS, Walter P.** 2000. Functional and genomic analyses reveal an essential coordination between the unfolded protein response and ER associated degradation. Cell **101:**249-258.
7. **Ron D, Walter P.** 2007. Signal integration in the endoplasmic reticulum unfolded protein response. Nat Rev Mol Cell Biol **8:**519-529.
8. **Horibe T, Hoogenraad NJ.** 2007. The chop gene contains an element for the positive regulation of the mitochondrial unfolded protein response. PloS one **2:**e835.
9. **Ron D, Habener JF.** 1992. CHOP, a novel developmentally regulated nuclear protein that dimerizes with transcription factors C/EBP and LAP and functions as a dominant-negative inhibitor of gene transcription. Genes Dev **6:**439-453.
10. **Song B, Scheuner D, Ron D, Pennathur S, Kaufman RJ.** 2008. Chop deletion reduces oxidative stress, improves beta cell function, and promotes cell survival in multiple mouse models of diabetes. J Clin Invest **118:**3378-3389.

11. **Tabas I, Ron D.** 2011. Integrating the mechanisms of apoptosis induced by endoplasmic reticulum stress. Nat Cell Biol **13:**184-190.

12. **Habib SJ, Waizenegger T, Neiewienda A, Paschen SA, Neupert W, Rapaport D.** 2007. The N-terminal domain of Tob55 has a receptor-like function in the biogenesis of mitochondrial b-barrel proteins. J Cell Biol **176:**77-88.

13. **Schnell DJ, Hebert DN.** 2003. Protein translocations: multifunctional mediators of protein translocation across membranes. Cell **112:**491-505.

14. **Koehler CM.** 2004. New developments in mitochondrial assembly. Annu Rev Cell Dev Biol **20:**309-335.

15. **Rehling P, Brandner K, Pfanner N.** 2004. Mitochondrial import and twin-pore translocase. Nat Rev Mol Cell Biol **5:**519-530.

16. **Bose HS, Lingappa VR, Miller WL.** 2002. Rapid regulation of steroidogenesis by mitochondrial protein import. Nature **417:**87-91.

17. **Pawlak KJ, Prasad M, Thomas JL, Whittal RM, Bose HS.** 2011. Inner mitochondrial translocase Tim50 interacts with 3beta-hydroxysteroid dehydrogenase type-2 to regulate adrenal and gonadal steroidogenesis. J Biol Chem **286:**39130-39140

18. **Rajapaksha M, Kaur J, Prasad M, Pawlak KJ, Marshall B, Perry EW, Whittal RM, Bose HS.** 2016. An outer mitochondrial translocase, Tom22, is crucial for inner mitochondrial steroidogenic regulation in adrenal and gonadal tissues. Mol Cell Biol **36:**1032-1047.

19. **van Wilpe S, Ryan MT, Hill K, Maarse AC, Meisinger C, Brix J, Dekker PJ, Mocsko M, Wagner R, Meijer M, Guiard B, Honlinger A, Pfanner N.** 1999. Tom22 is a multifunctional organizer of the mitochondrial preprotein translocase. Nature **401:**485-489.

20. **Yamaguchi H, Wang H-G.** 2004. CHOP is involved in Endoplasmic Reticulum stress-induced apoptosis by enhancing DR5 expression in human carcinoma cells. J Biol Chem **279:**45496-45502.

21. **Bose M, Debnath D, Chen Y, Bose HS.** 2007. Folding, activity and import of steroidogenic acute regulatory protein (StAR) into mitochondria changed by nicotine exposure. J Mol Endocrinol **39:**67-79.

22. **Bose M, Whittal RM, Miller WL, Bose HS.** 2008. Steroidogenic activity of StAR requires contact with mitochondrial VDAC1 and phosphate carrier protein. J Biol Chem **283:**8837-8845.

23. **Prasad M, Thomas JL, Whittal RM, Bose HS.** 2012. Mitochondrial 3-beta hydroxysteroid dehydrogenase enzyme activity requires a reversible pH-dependent conformational change at the intermembrane space J Biol Chem **287:**9534-9546.

24. **Gill SC, von Hippel PH.** 1989. Calculation of protein extinction coefficients from amino acid sequence data. Anal Biochem **182:**319-326.

25. **Pawlak KJ, Prasad M, McKenzie KA, Wiebe JP, Gairola CG, Whittal RM, Bose HS.** 2011. Decreased cytochrome c oxidase IV expression reduces steroidogenesis. J Pharmacol Exp Ther **338:**598-604.

26. **Bairoch A, Apweiler R.** The SWISS-PROT protein sequence database and its supplement TrEMBL in 2000. Nucleic Acid Res **28:**45-48.

27. **Pletnev VZ, Thomas JL, Rhaney FL, Holt LS, Scaccia LA, Umland TC, Duax WL.** 2006. Rational proteomics V: Structure-based mutagenesis has revealed key residues responsible for substrate recognition and catalysis by the dehydrogenase and isomerase activities in human 3β-hydroxysteroid dehydrogenase/isomerase type 1. J Steroid Biochem Mol Biol **101:**50-60.

28. **Rajapaksha M, Prasad M, Thomas JL, Whittal RM, Bose HS.** 2013. 3-beta hydroxysteroid dehydrogenase2 (3βHSD2) requires chaperone-assisted folding for steroidogenic activity. ACS Chemi Biol **8:**1000-1008.

29. **Krieger E, Darden T, Nabuurs SB, Finkelstein A, Vriend G.** 2004. Making optimal use of empirical energy functions: force-field parameterization in crystal space. Proteins**:**678-683.

30. **Vriend G.** 1990. WHAT IF: A molecular modeling and drug design program. J Mol Graph **8:**52-56.

31. **Jones DT.** 1999. Protein secondary structure prediction based on position-specific scoring matrices. J Mol Biol **292:**195-202.

32. **Hooft RW, Vriend G, Sander C, Abola EE.** 1996. Errors in protein structures. Nature **381:**272.

33. **Bowie JU, Lüthy R, Eisenberg D.** 1991. A method to identify protein sequences that fold into a known three-dimensional structure. Science **253:**164-170.

719 34. **Lüthy R, Bowie JU, Eisenberg D.** 1992. Assessment of protein models with three-dimensional
720 profiles. Nature **356:**83-85.

721 35. **Ramachandran GN, Ramakrishnan C, Sasisekharan V.** 1963. Stereochemistry of polypeptide chain
722 configurations. J Mol Biol **7:**95-99.

723 36. **Hooft RW, Sander C, Vriend G.** 1997. Objectively judging the quality of a protein structure from a
724 Ramachandran plot. Comput Appl Biosci **13:**425-430.

725 37. **Liu H, Elstner M, Kaxiras E, Frauenheim T, Hermans J, Yang W.** 2001. Quantum mechanics
726 simulation of protein dynamics on long timescale. Proteins **44:**484-489.

727 38. **Ni M, Lee AS.** 2007. ER Chaperone in mammalian development and human diseases. FEBS Lett
728 **581:**3641-3651.

729 39. **Vance JE.** 1990. Phospholipid synthesis in a membrane fraction associated with mitochondria. J Biol
730 Chem **265:**7248-7256.

731 40. **Donzeau M, Kaldi K, Adam A, Paschen S, Wanner G, Guiard B, Bauer MF, Neupert W,**
732 **Brunner M.** 2000. Tim23 links the inner and outer mitochondrial membranes. Cell **101:**401-412.

733 41. **Rimmer KA, Foo JH, Ng A, Petrie EJ, Shilling PJ, Perry AJ, Mertens HD, Lithgow T, Mulhern**
734 **TD, Gooley PR.** 2011. Recognition of mitochondrial targeting sequences by the import receptors
735 Tom20 and Tom22. J Mol Biol **405:**804-818.

736 42. **Schneider H-C, Westermann B, Neupert W, Brunner M.** 1996. The nucleotide exchange factor
737 MGE exerts a key function in the ATP-dependent cycle of mt-HSP70-Tim44 interaction driving
738 mitochondrial protein import. EMBO J **15:**5796-5803.

739 43. **de Backer M, McSweeney S, Rasmussen HB, Riise BW, Lindley P, Hough E.** 2002. The 1.9 A
740 crystal structure of heat-labile shrimp alkaline phosphatase. J Mol Biol **318:**1265-1274.

741 44. **Kim EE, Wyckoff HW.** 1991. Reaction mechanism of alkaline phosphatase based on crystal
742 structures. two-metal ion catalysis. J Mol Biol **218:**449-464.

743 45. **Blom N, Gammeltoft S, Brunak S.** 1999. Sequence- and structure-based prediction of eukaryotic
744 protein phosphorylation sites J Mol Biol **294:**1351-1362.

46. **Rajapaksha M, Thomas JL, Streeter M, Prasad M, Whittal RM, Bell JD, Bose HS.** 2011. Lipid-mediated unfolding of 3-beta hydroxysteroid dehydrogenase2 is essential for steroidogenic activity. Biochemistry **50:**11015-11024.

47. **Hayashi T, Su TP.** 2007. Sigma-1 receptor chaperones at the ER-Mitochondrion interface regulate Ca2+ signaling and cell survival. Cell **131:**596-610.

48. **Molinari M.** 2007. N-glycan structure dictates extension of protein folding or onset of disposal. Nat Chem Biol **3:**313-320.

49. **Ma Y, Hendershot L.** 2004. The role of the unfolded protein response in tumour development: friend or foe? Nat Rev Cancer **4:**966-977.

50. **Kincaid MM, Cooper AA.** 2007. Misfolded proteins traffic from the endoplasmic reticulum (ER) due to ER export signals. Mol Biol Cell **18:**455-463.

51. **Kornmann B, Currie F, Collins SR, Schuldiner M, Nunnari J, Weissman JS, Walter P.** 2009. An ER-Mitochondria tethering complex revealed by a synthetic biology screen. Science **325:**477-481.

52. **Giorgioa V, von Stockuma S, Antonielb M, Fabbrob A, Fogolaric F, Forted M, Glicke GD, Petronillia V, Zorattia M, Szabóf I, Lippeb G, Bernardi P.** 2013. Dimers of mitochondrial ATP synthase form the permeability transition pore. Proc Natl Acad Sci USA **110:**5887-5892.

53. **Komarov AG, Deng D, Craigen WJ, Colombini M.** 2005. New insights into the mechanism of permeation through large channels. Biophys J **89:**3950-3959.

765 **FIGURE LEGENDS**

766 **Figure 1.** Effect of stress on adrenal steroid synthesis. (A) Schematic presentation of steroid biosynthesis.
767 StAR is synthesized upon stress and hormonal stimulation, but CHOP is expressed only on stress. After
768 reaching near the outer mitochondrial membrane, StAR facilitates fostering cholesterol from the outer to inner
769 mitochondria to initiate steroid synthesis. (B) Schematic presentation of localization of different membrane
770 associated proteins, which are part of the MAM fraction present in the cytoplasm. A possible role of the outer
771 and inner mitochondrial translocases and their interaction with steroidogenic proteins is clearly described. (C)
772 Protein expression in the adrenal glands of mice with or without exposure to stress. The adrenal glands were
773 isolated immediately following the last period of stress, and proteins were analyzed by Western blotting with
774 the indicated antibodies. Mouse Leydig MA-10 cells were serum starved and cell lysates were used as a
775 control. (D) Measurement of ^{14}C-cholesterol to ^{14}C-pregnenolone conversion by mitochondria isolated from
776 the adrenal glands of the experimental animals. The metabolic reactions were initiated with NADPH at 37˚C.
777 Trilostane (Tril) was applied as an inhibitor of 3βHSD2 activity. The right panel shows a quantitative estimate
778 of the amount of pregnenolone synthesized from the metabolic reactions. The bottom panels show the Western
779 blots of the mitochondrial lysates stained with VDAC2 and 3βHSD2 independently. (E) ^{3}H-Pregnneolone to
780 ^{3}H-progesterone conversion by adrenal mitochondria isolated from animals with and without exposure to stress.
781 The metabolic reaction was initiated with NAD and Trilostane (Tril) was applied as an inhibitor of 3βHSD2
782 activity. The right panel shows a quantitative estimate of the amount of progesterone synthesized from the
783 metabolic reactions. The bottom panels show the Western blots of the mitochondrial lysates stained with
784 VDAC2 and 3βHSD2 independently. (F) Analysis of the change in serum corticosterone synthesis before and
785 after stress. The serum corticosterone increased from 1.4 ng/ml to 1.68 ng/ml following stress ($p \leq 0.0003$).
786 Data in panels D-F are the mean ±SEM of at least three independent experiments performed at three different
787 times.

788 **Figure 2.** CHOP expression impacts 3βHSD2-Tom22-VDAC2 interaction. (A) Left, siRNA mediated CHOP
789 knockdown. Right, Crude mitochondria were isolated from the wild-type MA-10 and ΔCHOP MA-10 cells,
790 solubilized in digitonin, analyzed through 4-16% native gradient PAGE and stained with 3βHSD2 antibody.
791 The left bottom panel show equal 3βHSD2 levels from the mitochondria applied in each reaction. (B - D) Co-

immunoprecipitation of the digitonin-solubilized lysate from adrenal mitochondria of wild-type mice without (B) and with stress (C), and CHOP-null mice with stress (D). In all control lanes (First lanes in B-D) lysate from stressed animal adrenals were applied. The immunocomplexes were isolated using the indicated antibodies and then stained with 3βHSD2, Tom22, VDAC2, and CHOP antibodies independently. (E) Expression of 3βHSD2, VDAC2, HSP70, StAR, GRP78, calnexin (cal) and CHOP by the wild-type and CHOP-null adrenals with and without stress by Western blotting. Nonsteroidogenic COS-1 cells were applied to show its difference from MA-10 cells. Serum starved MA-10 cell lysate was used as control. (F) Measurement of ATP release by mitochondria isolated from wild-type and ΔCHOP MA-10 cells after incubation with various concentrations of mCCP. (G) Percoll density distribution analysis of the subcellular localization of CHOP, 3βHSD2 and VDCA2 after stress. (H) Modeling of Tom22 and analysis of its membrane association. A computer model structure of Tom22 showing its extremely flexible nature with the maximum unstructured region and the absence of sheets. (I) The space filling model of Tom22 showing its organization within the OMM. (J) Helical organization of the amino acids present in the Tom22 model shown in panel H. Data in panel F is the mean ±SEM of at least three independent experiments performed at three different times.

Figure 3. Domains mediating 3βHSD2-Tom22 interaction. (A) Expression of the Tom22 L2 loop region mutants, D35A, D37S, E39A and 35-39 Mut, in ΔTom22 cells. The scrambled siRNA was used as a negative control (Neg siRNA). The top panel shows the quantitative expression level of the Tom22 mutants. Bottom, VDAC2 expression remained unchanged. (B) Fractionation of the mitochondrial compartments of MA-10 cells and staining with the indicated antibodies either in combination or independently. The import fragment was proteolyzed by proteinase K (PK). (C) Mitochondrial fractionation of ΔTom22 MA-10 cells following expression of the indicated mutants and staining with Tom22, VDAC2, Tim23 and COX-IV antibodies independently. (D) Immunoelectron microscopy of the Tom22 (red arrows) independently or with 3βHSD2 (blue arrows) as indicated. (E) Immunoelectron microscopy of ΔTom22 cells after expression of the indicated mutants (red arrows) and then colocalization with 3βHSD2 (blue arrows). The bottom panels are enlarged images of representative mitochondria from the same experiment indicated above. (F) Metabolic conversion of ^{3}H-pregnenolone to ^{3}H-progesterone by ΔTom22 cells expressing the indicated Tom22 mutants and initiated with NAD. Trilostane (Tril) was applied as a negative control, and Neg siRNA was applied to show the

specificity of the Tom22 siRNA. The top panel shows the quantitative measurement of the progesterone synthesized. (G) Metabolic conversion of cholesterol to pregnenolone by ΔTom22 cells expressing the indicated Tom22 mutants. The top panel shows a quantitative estimation of the amount of pregnenolone synthesized in the bottom panel. (H) Co-immunoprecipitation of the Tom22 mutants and Western staining with Tom22, 3βHSD2 and VDAC2 antibodies independently. Reprobing the same membrane with VDAC2 indicates equal amount of protein present in each lane. Data in panels A, F and G are the mean ±SEM of at least three independent experiments performed at three different times.

Figure 4. Specificity of IMS resident amino acids. (A) Expression of the H8 and L8 loop region mutants, Q118L, N124K, T125I, M131R and A134D, in ΔTom22 cells. The scrambled siRNA was used as a negative control. Bottom, VDAC2 expression remained unchanged. (B) Mitochondrial fractionation of ΔTom22 cells after expression of the indicated mutants and analysed after staining with Tom22, VDAC2, Tim23 and COX-IV antibodies independently. (C) Immunoelectron microscopy of the ΔTom22 cells following expression of the mutants (red arrows) and their colocalization with 3βHSD2 (blue arrows). The bottom panels are enlarged images of representative mitochondria from the same experiment indicated above. (D) ^{3}H-Pregnenolone to ^{3}H-progesterone conversion following expression of the indicated mutants and initiation with NAD. Trilostane was applied as a negative control, and the Neg siRNA was applied to show the specificity of the Tom22 siRNA. The top panel is the quantitative estimation of the amount of steroid synthesized. (E) Co-immunoprecipitation of the indicated Tom22 mutants with Tom22, 3βHSD2 and VDAC2 antibodies independently. 3βHSD2 antibody staining on longer exposure is also presented just bottom of the 3βHSD2 panel and shown by a curved arrow. Data in panel D is the mean ±SEM of at least three independent experiments performed at three different times.

Figure 5. Analysis of cellular architecture by immunohistochemistry. (A) Sections of wild-type (left panels) and CHOP null (right panels) adrenal glands probed by immunhistochemical staining for the expression of Tom22 (panels a and b); StAR (panels c and d); 3βHSD2 (panels e and f); aldosterone synthase (panels g and h); VDAC2 (panels i and j). The cells contain intracytoplasmic lipid stores. Aldosterone synthase immunoreactivity was localized in the Zona Glomerulosa of both specimens (panels g and h). The remainder of

the panels shows findings from the Zona Fasciculata of the two specimens (hematoxylin counterstain, original magnification: X400). (B) The identical preparations at X1000 magnification from the panel A. The pattern of immunoreactvity is cytoplasmic for all antigens in both specimens. (C) Electron microscopy of adrenals from wild-type and CHOP -/- mice stained with Tom22 without and with 3βHSD2. The top panels show the enlarged view of mitochondria.

Figure 6. Role of phosphates in steroid synthesis. (A) Serum phosphate levels in wild-type and CHOP -/- mice exposed to stress as compared with controls. The serum phosphate of the wild-type mice was increased from 6.2 mM to 7.4 mM ($p \leq 00029$) following stress but CHOP null mice had no difference ($p \leq 0.153$) before and after stress. (B) ^{3}H-Pregneolone to ^{3}H-progesterone conversion by mitochondria isolated from MA-10 cells incubated with 3βHSD2 and various NaH_2PO_4 concentrations, ranging from 0 to 100 mM. The top panel shows the quantitative measurement of the amount of steroid synthesized. The bottom panel shows that equal amounts of mitochondria were employed. (C) ^{3}H-Pregneolone to ^{3}H-progesterone conversion by MA-10 cell mitochondria with 3βHSD2 preincubated with Tris (pH 7.4) for phosphate removal. In some cases, mitochondria or 3βHSD2 were preincubated with Tris buffer. The quantitative estimation is presented in the top. (D) Similar metabolic conversion after dephosphorylation of 3βHSD2 with varying amounts of SAP and then restoring activity after incubation with 100 mM NaH_2PO_4. Quantitative measurements are shown in the right panel. The bottom panels, C and D, were stained with VDAC2 antibody showing same amount of mitochondrial protein was applied in each reaction. (E) The model, regenerated by Pymol molecular graphics with the solvent preset, shows the presence of six β-sheets numbered 1-6. The protein structure of 3βHSD2 shows 12 segments of residues (15−26, 43−56, 66−75, 88−93, 96−115, 154−174, 191−200, 202−207, 225−238, 245−253, 331−335, and 346−360) that form 12 α-helices, shown as α1- α12, and six segments of residues (1−7, 31−36, 57−60, 78−82, 181−183, and 264−266) that form six β-sheets, shown as β1-β6. In the solvent view structure of 3βHSD2, the residues for the α-helices are shown in different colors depending on their location. (F, G) Determination of the activity of the 3βHSD2 mutants to define possible role of serine residues. (H, I) Determination of activity (H) and expression (I) of the 3βHSD2 mutants after transfection in nonsteroidogenic COS-1 cells. VDAC2 expression shows the equivalent loading in each lane. Data presented in

panels A-D,F and G are the mean ±SEM of at least three independent experiments performed at three different times.

Figure 7. Role of phosphate in 3βHSD2 stabilization. (A) Native gradient PAGE of the digitonin solubilized complex stained with a 3βHSD2 antibody from the mitochondria isolated from steroidogenic cells deprived of phosphate followed by external addition of 5, 15, 30 and 100mM sodium phosphate. (B) An analysis of the 3βHSD2-containing 450 kDa complex from the phosphate deprived cells followed by addition of indicated concentrations of phosphate. (C) Similar native gradient PAGE of the digitonin-solubilized complex from MA-10 mitochondria after external addition of sodium phosphate in the absence of phosphate deprivation. (D) A comparative analysis of the 450 kDa native complex intensity by external addition of phosphate. (E) Thermal unfolding of the dephosphorylated (purple line) and untreated (black line) 3βHSD2 recorded in a CD spectropolarimeter at 222 nm from 4˚C to 90˚C. (F) Thermal unfolding of 3βHSD2 recorded in a CD spectropolarimeter at 222 nm from 4˚C to 90˚C with two different concentrations of sodium ions, 1.0M (blue line) and 10mM (black line) NaH_2PO_4, pH 7.4. (G) Schematic presentation explaining the stability of 3βHSD2 with and without phosphate. The wild-type is in a native state "N" and upon gradual thermal denaturation; it forms an intermediate denaturation "Iu" generating thermal unfolding "Tm/Pu" at 33˚C with a pseudo plateau at 41˚C. Then, 3βHSD2 goes through a two-step unfolding process with a Tm of 47˚C and final denaturation "D". In the case of the phosphate-preincubated protein, the protein undergoes a two-step unfolding with a Tm of 52˚C. Data in panels C and D represent the mean ±SEM of at least three independent experiments performed at three different times.

Table Legends

Table 1 and 3. Proteins in the 750-kDa 3βHSD2-containing complex isolated from WT (1) and CHOP knockdown (3) MA-10 cells following native gradient PAGE (4-16%) and mass spectrometry. The common molecules between the 750 and 550 kDa complex of the MA-10 cells are in italics and the CHOP knockdown MA-10 cells are indicated in italics with underlined.

Table 2 and 4. Proteins in the 550-kDa 3βHSD2-containing complex isolated from WT (2) and CHOP knockdown (4) MA-10 cells following native gradient PAGE (4-16%) and mass spectrometry.

898

899

Molecular and Cellular Biology

900

Table 1 (MA-10 750 kDa native complex)

Accession No.	Protein	MS/MS Score	No. of unique peptides
26984237	mitochondrial ATP-dependent protease Lon	1959	29
344268714	*60 kDa heat shock protein, mitochondrial*	1319	31
6755967	*voltage-dependent anion-selective channel protein 3 isoform 2*	589	9
19745150	*NADH-cytochrome b5 reductase 3*	570	11
73987072	lon protease homolog, mitochondrial isoform 1	527	10
154816168	stress-70 protein, mitochondrial	527	7
351694722	*Aldehyde dehydrogenase, mitochondrial*	314	9
351708365	*NADH-cytochrome b5 reductase 3*	256	5
726095	long-chain acyl-CoA dehydrogenase	181	3
149410696	*voltage-dependent anion-selective channel protein 3-like isoform 1*	179	4
31542438	*cytochrome b5 type B precursor*	265	4
340546142	*voltage-dependent anion channel 1*	136	4
9910382	mitochondrial import receptor subunit TOM22	132	3
345305898	*voltage-dependent anion-selective channel protein 2-like isoform 1*	126	2
47058986	mitochondrial import receptor subunit TOM40	119	2
13385998	heat shock protein 75 kDa, mitochondrial precursor	115	3
301070250	hydroxyacyl-Coenzyme A dehydrogenase	110	2
339243731	ADP/ATP translocase 1calcium binding 140k protein	78	21
16758454	phosphatidate cytidylyltransferase 2	64	1

901

Table 2 (MA 10 550 kDa native complex**)**

Accession No.	Protein	MS/MS Score	No. of unique peptides
194044029	*60 kDa heat shock protein, mitochondrial*	1066	23
238427	Porin 31HM	561	9
297265430	protein disulfide-isomerase A6 isoform 1	368	6
6755967	*voltage-dependent anion-selective channel protein 3 isoform 2*	335	7
225706314	*Voltage-dependent anion-selective channel protein 2*	287	7
860986	protein disulfide isomerase	254	5
307199045	*60 kDa heat shock protein, mitochondrial*	252	7
340546142	*voltage-dependent anion channel 1*	144	3
109075624	membrane-associated progesterone receptor component 2	118	1
297272126	*fatty aldehyde dehydrogenase isoform 6*	110	2
12055497	Ca2+-ATPase 1	109	1
386758	GRP78 precursor	97	2
550062	GTP-binding protein	93	2
2414516	surface 4 integral membrane protein	76	2
2662291	*cytochrome b5*	76	1
553254	*NADH cytochrome b5 reductase*	71	2

902
903

904

Table 3 (ΔCHOP MA-10 750 kDa native complex**)**

Accession No.	Protein	MS/MS Score	No. of unique peptides
51455	*heat shock protein 65*	969	19
344268714	60 kDa heat shock protein, mitochondrial	882	16
6753036	*aldehyde dehydrogenase, mitochondrial precursor*	875	16
4105605	*voltage dependent anion channel*	270	5
726095	*long-chain acyl-CoA dehydrogenase*	250	5
386758	*GRP78 precursor*	202	4
5733504	*voltage-dependent anion channel VDAC3*	131	3
205632	*Na,K-ATPase alpha-1 subunit*	114	2
247307	*cytochrome P450 reductase*	99	2
118596522	*acetaldehyde dehydrogenase*	89	2
199599757	protein disulfide isomerase-associated 3 precursor	83	2
147898791	ADH-cytochrome b5 reductase 2 precursor	71	1
4566870	malate dehydrogenase	68	1
225706314	Voltage-dependent anion-selective channel protein 2	57	3

905
906

907

Table 4 (ΔCHOP MA-10 550 kDa native complex**)**

Accession No.	Protein	MS/MS Score	No. of unique peptides
116089322	lon protease homolog, mitochondrial precursor	1681	25
51455	*heat shock protein 65*	1442	26
6753036	*aldehyde dehydrogenase, mitochondrial precursor*	1142	23
147900646	heat shock 70kDa protein 9	500	8
355762276	*78 kDa glucose-regulated protein*	471	9
63018	beta-actin	464	9
205632	*Na,K-ATPase alpha-1 subunit*	449	7
726095	*long-chain acyl-CoA dehydrogenase*	436	7
6679421	*NADPH--cytochrome P450 reductase*	409	7
4105605	*voltage dependent anion channel*	304	6
13385998	heat shock protein 75 kDa, mitochondrial precursor	271	4
31542438	cytochrome b5 type B precursor	228	5
5733504	*voltage-dependent anion channel VDAC3*	207	3
212653	Ca2+ ATPase	192	4
158422314	molecular chaperone DnaK	153	3
124245114	*glucose-regulated protein 78*	130	4
56188	glyceraldehyde 3-phosphate-dehydrogenase	123	2
340546142	voltage-dependent anion channel 1	117	3
118596522	*acetaldehyde dehydrogenase*	83	2
348500154	isocitrate dehydrogenase [NAD] subunit alpha	73	1

908